https://doi.org/10.5194/gmd-2020-258
Preprint. Discussion started: 22 September 2020

Geoscientific Model Development Discussions

Ecosystem age-class dynamics and distribution in the LPJ-wsl v2.0 global ecosystem model

Leonardo Calle[1,2] and Benjamin Poulter[3]

Correspondence to: Leonardo Calle (leonardo.calle@umontana.edu)

1 University of Montana, Department of Forest Management, WA Franke College of Forestry and Conservation, Missoula, MT 59812

2 Montana State University, Department of Ecology, Bozeman, Montana 59717, USA

3 NASA Goddard Space Flight Center, Biospheric Science Laboratory, Greenbelt, Maryland 20771, USA

Correspondence to: Leonardo Calle (leonardo.calle@umontana.edu)

Abstract. Forest ecosystem processes follow classic responses with age, peaking production around canopy closure and declining thereafter. Although age dynamics might be more dominant in certain regions over others, demographic effects on net primary production (NPP) and heterotrophic respiration (Rh) are bound to exist. Yet, explicit representation of ecosystem demography is notably absent in most global ecosystem models. This is concerning because the global community relies on these models to regularly update our collective understanding of the global carbon cycle. This paper aims to fill this gap in understanding by presenting the technical developments of a computationally-efficient approach for representing age-class dynamics within a global ecosystem model, the LPJ-wsl v2.0 Dynamic Global Vegetation Model. The modeled age-classes are initially created by fire feedbacks, wood harvesting, and abandonment of managed land, otherwise aging naturally until a stand-clearing disturbance is simulated or prescribed. In this paper, we show that the age-module can capture classic demographic patterns in stem density and tree height compared to inventory data, and that patterns of ecosystem function follow classic responses with age. We also present a few scientific applications of the model to assess the modeled age-class distribution over time and to determine the demographic effect on ecosystem fluxes relative to climate. Simulations show that, between 1860 and 2016, zonal age distribution on Earth was driven predominately by fire, causing a ~45-year difference in ages between boreal (50N-90N) and tropical (23S-23N) latitudes. Land use change and land management was responsible for an additional decrease in zonal age by -6 years in boreal and by -21 years in temperate (23N-50N) and tropical latitudes, with the anthropogenic effect on zonal age distribution increasing over time. A statistical model helped reduced LPJ-wsl v2.0 complexity by predicting per-grid-cell annual NPP and Rh fluxes by three terms: precipitation, temperature and age-class; at global scales, R^2 was between 0.95 and 0.98. As determined by the statistical model, the demographic effect on ecosystem function was often less than 0.10 kg C m^{-2} yr^{-1} but as high as 0.60 kg C m^{-2} yr^{-1} where the effect was greatest. In eastern forests of North America, the demographic effect was of similar magnitude, or greater than, the effects of climate; demographic effects were similarly important in large regions of every vegetated continent. Spatial datasets are provided for global ecosystem ages and the estimated coefficients for effects of precipitation, temperature and demography on ecosystem function. The discussion focuses on our finding of an increasing role of demography in the global carbon cycle, the effect of demography on relaxation times (resilience) following a disturbance event and its implications at global scales, and a finding of a 40-Pg C increase in turn-

https://doi.org/10.5194/gmd-2020-258
Preprint. Discussion started: 22 September 2020

over from age dynamics at global scales. Whereas time is the only mechanism that increases ecosystem age, any additional disturbance not explicitly modeled will decrease age. The LPJ-wsl v2.0 age-module therefore simulates the upper limit of age-class distributions on Earth and represents another step forward towards understanding the role of demography in global ecosystems.

1 Introduction

Forest ecosystem production follows predictable patterns with time since disturbance – the classic forest age-production curves from Odum (1969), where net ecosystem production (NEP) peaks around canopy closure, declining thereafter due to hydraulic limitations on gross primary production (Ryan et al. 2004, Drake et al. 2010, 2011), increases in heterotrophic respiration from biomass turnover, as well as from stand-level declines in population density (Ptrezsch and Biber 2005, Stephenson et al. 2014). That younger forests are more productive than older forests has been long-standing knowledge in forestry, as evidenced by yield and growth tables dating back to the 18^{th} Century that incorporated stand age into their calculations of lumber production (Pretzsch et al. 2008).

On global scales, forest age is a considerable factor in global carbon cycling. Regrowth following disturbance comprises ~60% of the total land carbon sink based on country-level forest inventories (Pan et al. 2011a; tropical regrowth sink of 1.6 ± 0.5 Pg C yr^{-1}) and model-based studies (Pugh et al. 2019a; global regrowth sink of 0.3 to 1.1 Pg C yr^{-1}). In the last decade, explicit model representation of forests as a function of time since disturbance (hereafter simply, 'ecosystem age') has been a grand challenge in an effort to quantify the demographic response of forests to changes in climate, atmospheric CO_2, disturbances (Friend et al. 2014, Kondo et al 2018, Pugh et al. 2019a), fire, and land use change and land management (LUCLM) (Gitz and Ciais 2003, *Model*: OSCAR; Shevliakova et al. 2009, *Model*: LM3V; Haverd et al. 2014, *Model*: CABLE-POP; Lindeskog et al. 2013, *Model*: LPJ-GUESS; Yue et al. 2018, *Model*: ORCHIDEE MICT; Nabel et al. 2019, *Model*: JSBACH4; Longo et al. 2019, *Model*: ED-2.2). Much of the focus of these global modeling studies has been on the effect of natural and anthropogenic disturbances on the carbon dynamics in old-growth versus second-growth forests (Gitz and Ciais 2003, Shevliakova et al. 2009, Kondo et al 2018, Yue et al. 2018, Pugh et al. 2019a), lacking finer distinction of demographic effects, for example, when age-classes near canopy closure have the greatest NEP.

Both large-scale (> 0.1 ha) natural and anthropogenic ecosystem disturbances that reset ecosystem age can be generally ranked in the following order according to global area disturbed: fire > windstorms > forest management > shifting cultivation (Frolking et al. 2009). Much of the evidence for the relative importance and global distribution of large disturbances has come from either satellite retrievals of spectral indices indicating forest loss or burn scars on the land (Potter et al. 2003, Frolking et al. 2009, Pugh et al. 2019b), national forest inventory records of land use change and forest management (Houghton 1999, FAO-FRA 2015, Williams et al. 2016), or from model-based studies (Goldewijck 2001, Arneth et al. 2017) that integrate information on historical land use (Goldewijck 2001, Hurtt et al. 2006). Other natural disturbances such as pest and pathogen outbreaks, flooding, ice storms, and volcanic erup-

https://doi.org/10.5194/gmd-2020-258
Preprint. Discussion started: 22 September 2020

Geoscientific Model Development Discussions

tions are less widespread globally (Frolking et al. 2009) but are still influential drivers of landscape patch dynamics (Dale et al. 2001, Turner 2010). In the coterminous United States, forest management is the predominant forest disturbance (1.4% of forested area converted to non-forest and then re-established annually), followed by fire (0.01-0.5% of forested area burned annually 1997-2008) (Williams et al. 2016). Although pest and pathogens, namely bark beetle infestations, affected a much larger area (up to 6% of total forested area in U.S.) than both logging and fire, the effects do not always cause stand replacement. It is arguable whether fire and forest management are the two most important global drivers of ecosystem age (Pan et al. 2011b), but nevertheless these are the drivers applied in a model framework in this study, in a manner that moves modeling one step forward to assess global age-class dynamics.

The overall aim of this study was to fill a gap in existing knowledge by simulating the time-evolution of age-class distributions in a global ecosystem model and to determine if explicit representation of demography influenced ecosystem stocks and fluxes at global scales or at the level of a grid-cell. Technical details are presented for a module representing age-class dynamics, driven by fire feedbacks, land abandonment and wood harvesting in the Lund Potsdam Jena (LPJ-wsl; Sitch et al. 2003) Dynamic Global Vegetation Model (DGVM). Analyses are presented of model behavior, in terms of age-structure and age-functional patterns, the temporal evolution of age distributions and their causative drivers, and a statistical model of ecosystem production and respiration as a function of demography and climate.

2 Methods

2.1 LPJ-wsl v2.0 General Model Description

2.1.1 LPJ History

LPJ-wsl v2.0 has its legacy in the LPJ family of models, first developed by Sitch et al. (2003) in a Fortran coding environment [1]. In 2007, Bondeau et al. (2007) produced the LPJmL codebase, in C, which included the addition of 'managed lands'. The model known as LPJ-wsl v2.0 is based on LPJmL v3.0, but includes modifications to managed lands that now includes modeling gross land cover transitions, forest age cohorts, and also a modification that include permafrost and wetland methane. Many developments were made in the publicly-available LPJmL4 (version 4.0; Schaphoff et al. 2018) that are not present in LPJ-wsl v2.0. The LPJ-wsl model was branched off of LPJmL sometime around 2010 and continued to diverge. In modern programming practices, the historical branching of parallel lines of model development would have been tracked with version control software. This research paper represents a large effort toward this end, and the LPJ-wsl v2.0 code is now freely and publicly available (https://github.com/benpoulter/LPJ-wsl_v2.0) under a GNU Affero General Public License version 3. LPJ-wsl v2.0, hereafter simply 'LPJ-wsl', excluding the version number unless an explicit reference is being made to prior versions or to clarify the version number.

1. LPJ and LPJmL History, https://www.pik-potsdam.de/research/projects/activities/biosphere-water-modelling/lpjml/history-1)

https://doi.org/10.5194/gmd-2020-258
Preprint. Discussion started: 22 September 2020

Geoscientific Model Development
Discussions

2.1.2 LPJ-wsl v2.0 Overview

LPJ-wsl v2.0 simulates soil hydrology and vegetation dynamics in 0.5˚ grid-cells, wherein climate, atmospheric CO_2, and soil texture is prescribed from driver datasets (Figure 1). Vegetation is categorized into Plant Functional Types (PFT; Box 1996). Plant populations compete for light, space, and soil water, depending on demand; nutrient cycles are not considered in this model version. LPJ-wsl is a 'big-leaf' ecosystem model, whereby leaf-level photosynthesis and respiration (Haxeltine and Prentice 1996, Farquhar et al. 1980) occur at daily time-steps, accounting for the photosynthetically active period (daytime), and is scaled to the stand-level using a mean-individual approximation, which assumes that important state variables (carbon stocks and fluxes) can be determined by using the average properties of a population. Plant populations are categorized using 10 PFTs in this study (phenology parameters and bioclimatic limits listed in SM Table 1); the same PFTs as in Sitch et al. (2003). Left unchanged are the PFT-specific bioclimatic limits, turnover rates, C:N tissue ratios, allometric ratios, and other parameters not explicitly commented on here, but as described in Sitch et al. (2003). Mortality occurs via reductions in population density if a PFT's annual carbon balance is less than zero or if fire occurs. The fire module and the representation of land use change and land management are described in detail in *Section 2.2.2*, as these modules require a greater number of modifications for integration with age-classes.

2.2 Age-class Module

2.2.1 An age-based model of ecosystems – sub-grid-cell patch dynamics

Age-classes are represented as sub-tiles within a grid-cell (Figure 1), which we refer to as 'patches'. Every patch has the same climate, atmospheric CO_2, and soil texture, but the properties of the patch, such as available soil water and light availability, are determined by feedbacks from plant demand within a patch; hereafter, 'age-class' and 'patch' are used interchangeably depending on context but describe the same entity. Plant processes (competition, photosynthesis, respiration) are simulated at the level of the patch for each PFT within the patch. The age-class module has a fixed number of age-classes that can be represented in a grid cell, but all age-classes are not always represented. In this setup, age-classes are classified into 12 age-classes (patches) in fixed age-width bins, defined as the *unequalbin* or the *10yr-equalbin* age-width setup (Table 1). The age-widths of the age-classes in the *10yr-equalbin* setup correspond to common age-widths of classes used in forest inventories. The *10yr-equal*bin age setup is used for all global simulations, whereas the *unequalbin* setup is applied to explore model dynamics at the level of a single grid-cell; simulation details in next section.

Age-classes are only created by fire, wood harvest, or land abandonment and are initialized to the youngest age-class. The fraction of the patch that burns gets its age 'reset' to the youngest age-class, 1-10 yr. The same process occurs for the fractional area that undergoes wood harvest or when managed land is abandoned and allowed to regrow – the fractional area undergoing an age-transition is reclassified as a 1-10 yr age-class. This process allows the model to accurately track the carbon stocks, fluxes and feedbacks associated with these state variables. For example, if a fire burns 50% of a patch, then 50% might have bare ground and 50% will have vegetation at pre-burn levels. If the probability of another fire is dependent on live vegetation, then feedbacks will result in a lower chance of fire on

https://doi.org/10.5194/gmd-2020-258
Preprint. Discussion started: 22 September 2020

the bare-ground fraction versus the fully-vegetated fraction that was not previously burned.

The most novel advancement in this study is a new method of age-class transition modeling, which we call 'vector-tracking of fractional transitions' (VTFT), which improves the computational efficiency of modeling age-classes in global models; this is a similar approach independently conceived by Nabel et al. (2019). The method is a transparent and simple solution to the problem of dilution, which manifests as an advective process when state variables, such as carbon stocks or tree density, are made to merge by area-weighted averaging. The concept of merging two unique model entities ('patch' or age-class) on the basis of similarity is a computational solution to constrain the number simulated patches in accordance with computer resources, but is also ecologically unrealistic. For example, along what axis of similarity is a patch considered to be most similar to another patch – in terms of PFT composition, biomass in plant organs, plant height, or stem density? Existing age-class models (Medvigy et al. 2009, *Model*: ED2; Lawrence et al. 2019, *Model*: CLMv5.0; Yu et al. 2018, *Model*: ORCHIDEE-MICT) employ merging rules (although some do not – Lindeskog et al. 2013, *Model*: LPJ-GUESS) with varying thresholds to ensure that patches are only merged if the difference among one state variable (biomass, tree height) is less than a fixed threshold. Merging rules along a single axis are arbitrary distinctions of similarity and VTFT circumvents these issues by not using merging rules at all. By design, VTFT allows age-classes to advance in a natural progression from young to old and ensures that age-class transitions always occur between the most similar age-classes along multiple state variables.

In matrix notation, VTFT describes a matrix of size (w := *agewidths per ageclass*, n := ageclasses), where the elements $f_{i,j}$ are the within-age-class fractional areas of the grid-cell:

$$\mathbf{F} = \begin{bmatrix} f_{1,1} & f_{1,2} & \cdots & f_{1,n} \\ f_{2,1} & f_{2,2} & \cdots & f_{2,n} \\ \vdots & \vdots & \ddots & \vdots \\ f_{w,1} & f_{w,2} & \cdots & f_{w,n} \end{bmatrix} = \left(f_{i,j} \in \mathbb{R}^{wxn}\right) \tag{1}$$

It is important to note here that within-age-class fractional areas ($f_{i,j}$) are only used during age-class transitions – this is a key point. For almost all calculations in LPJ, processes operate on the total fractional areas for each age-class, calculated by the total fractional area for each age-class,

$$\text{F\_total}_j = \sum_{i=1}^{w} f_{i,j} \tag{2}$$

, where F_total_j is the column sum of **F** for a given age-class (j); the calculation can be vectorized for efficiency by computing the dot product between an 'all-ones' row vector of length (w) and **F**. In practice, when LPJ-wsl simulates physical processes on an arbitrary carbon pool (C), for example, the calculations are computed on a per-mass basis, which then requires conversion to a per-area basis by multiplying the total carbon mass in an age-class by the representative total fractional area:

$$\mathrm{C_j}[\mathrm{kg\ m^{-2}}] = \mathrm{C_j}[\mathrm{kg}] \times \mathrm{F\_total_j} \tag{3}$$

, where C_j [*units* := kg or km^{-2}] is the total carbon for a given age-class (j). Again, the calculation can be computed via the Hadamard (element-wise) product, taking a vector ($\vec{C}$), where elements are the carbon pool totals for every age-class and multiplying by vector F_total, with elements of the total fractional areas in each age-class. In effect, all simulated processes in LPJ-wsl act on an area-basis, based on the column sums of **F**.

In every year of simulation, an age-class transition always occurs, and this procedure is defined as an operation that increments the positions of the elements as,

$$\mathbf{F}^{(t+1)} := \begin{bmatrix} f_{1,1}^{(t+1)} \stackrel{\text{def}}{=} f_{0,0}^{(t+1)} & f_{1,2}^{(t+1)} \stackrel{\text{def}}{=} f_{w,1}^{(t)} & \cdots & f_{1,n}^{(t+1)} \stackrel{\text{def}}{=} f_{w,n-1}^{(t)} \\ f_{2,1}^{(t+1)} \stackrel{\text{def}}{=} f_{1,1}^{(t)} & f_{2,2}^{(t+1)} \stackrel{\text{def}}{=} f_{1,2}^{(t)} & \cdots & f_{2,n}^{(t+1)} \stackrel{\text{def}}{=} f_{1,n}^{(t)} \\ \vdots & \vdots & \ddots & \vdots \\ f_{w,1}^{(t+1)} \stackrel{\text{def}}{=} f_{w-1,1}^{(t)} & f_{w,2}^{(t+1)} \stackrel{\text{def}}{=} f_{w-1,2}^{(t)} & \cdots & f_{w,n}^{(t+1)} \stackrel{\text{def}}{=} f_{w,n}^{(t)} + f_{w-1,n}^{(t)} \end{bmatrix} \tag{4}$$

, where the superscripts are the time indices for the current timestep (t+1) and the previous timestep (t), subscripts are the matrix indices, $f_{0,0}^{(t+1)}$ is the fractional area of a newly created stand (by definition, it is the youngest age-class fraction), and $f_{w,n}$ is the oldest fractional age of the grid-cell, which is incremented by an amount equal to fractional area ($f_{w-1,n}^{(t)}$). Of special importance is the bottom row of the **F** matrix, $F_{w,1\leq j\leq n}$, which are the fractional areas of each age-class transitioning to the next oldest age-class. The transitioning fractions (F_{w*}) become the incoming fractions in the next-oldest age-class. Using an arbitrary carbon pool (C) as an example, the carbon pool for the next timestep (t+1) would be calculated via an area-weighted average between the carbon remaining in the age-class and the carbon in the transitioning fraction,

$$\mathrm{C_j^{(t+1)}} = \frac{\left(\mathrm{C_j^{(t)}} \times \mathrm{F'\_total_j^{(t)}}\right) + \left(\mathrm{C_{j-1}^{(t)}} \times \mathrm{F_{w,j-1}^{(t)}}\right)}{\mathrm{F'\_total_j^{(t)}} + \mathrm{F_{w,j-1}^{(t)}}} \tag{5}$$

, where F'_total_j is the total fractional area of age-class (j) that remains in the age-class, $F_{w,j-1}^{(t)}$ is the transitioning or 'incoming' fraction from the younger age-class, and $C_{j-1}^{(t)}$ is the carbon pool (on area-basis, kg m^{-2}) in the younger age-class, calculated at the end of the previous timestep. Equation 5 effectively converts the units of the carbon pools from an area-basis (km m^{-2}) to a total mass (kg), taking the sum of the carbon remaining and transitioning into the age-class, and 'redistributes' the carbon mass by the new fractional area; during age-class transitions, these area-weighted averages are used to conserve mass across all state variables. In theory, VTFT minimizes the redistribution (or 'dilution') of mass across a larger area if the incoming fractional area is much smaller than the fractional area of the existing age-class.

In a plain-language summary of the matrix representation, VTFT ensures that a vector of fractional areas is associated with every age-class (n), of length (w), and where 'w' is equal to the age-width of the age-class, with elements (f) that are the fractional areas contributing to the total fractional area of the patch (*F_total*). When a young age-class

https://doi.org/10.5194/gmd-2020-258
Preprint. Discussion started: 22 September 2020

(a_1) is first created, VTFT vectors are initialized to zero and the first element (f_1) is set to the *incoming* fractional area. *Within-class Fractional Transitions*: For every simulation year, the position of each element (f_x) in the VTFT vector is incremented by the representative time of each element (x), which is simply 1. No changes occur to the state variables of the age-class during within-class transitions. *Between-class Fractional Transitions*: Upon incrementing the position of each element, if the value at (f_w) is non-zero, then the corresponding fractional area f_w, defined as the *outgoing* fraction, is used in an area-weighted average between the state variables of $a_1\, f_w$ and the next oldest age-class $a_2\, F\_total$. Lastly, upon incrementing element position, if all elements $< f_1 \ldots f_w >$ in the VTFT vector of the preceding age-class, in this example (a_1), are zeros, then the age-class is simply deleted from computational memory.

Two additional examples are provided in Figure 2 that demonstrate the procedure when there is a young age-class created, and another scenario when there are fractional age-class transitions between age-classes. With VTFT, any number of age-classes and age-widths can be modeled, but it is demonstrated that the age-widths employed in this study are sufficient to minimize the dilution of state variables when area-weighted averaging is used to merge fractional patches while also simulating stand-age patterns in state variables of carbon stocks, stem density and fluxes.

2.2.2 Integration with fire and land use change and land management (LUCLM) modules

Fire – The fractional area burned initiates the creation of a youngest age-class, or it gets merged with a youngest age-class if one exists already. Fire simulation is based on the semi-empirical Glob-FIRM model by Thonicke et al. (2001), with implementation details described in Sitch et al (2003). In short, fire is dependent on the length of the fire season, calculated as the number of dry days in a year above a threshold and a minimum fuel load, defined only as the mass of carbon in litter. When a fire occurs, PFT-specific fire resistances determine the fraction of the PFT population that gets burned. The biomass of burned PFTs, along with the aboveground litter in the patch, gets calculated as an immediate flux to the atmosphere. The fraction of the PFT population that does not burn maintains state variables (e.g., tree height, carbon in leaf and wood) at previous values; it is possible to have so called 'survivor' trees on the youngest age-class that then skews the age-height distribution of the patch. Fire occurs in both the primary forest and secondary forest tiles; the classification of primary versus secondary forests is determined by the land use driver dataset.

LUCLM – Age-classes get created when managed land is abandoned and allowed to regrow into secondary forests, or when wood harvest occurs on forested lands and causes deforestation. In both cases, the fractional area abandoned/logged initiates the creation of a youngest age-class, or it gets merged with a youngest age-class if one exists already. To improve accounting of primary forests, defined here as natural land without a history of LUCLM, and second-growth forests, defined as natural land with a history of LUCLM; transitions between these classes are unidirectional from primary -> secondary. In the LUCLM module, gross transitions between land uses (Pongratz et al. 2014, Stocker et al. 2014) are simulated, such that if the fraction of abandoned land equals the fraction of land deforested in the same year (net zero land use change), the fluxes from the gross transitions are tracked independently and gives an overall more accurate accounting (and higher magnitude) of emissions from LUC (Arneth et al. 2017).

https://doi.org/10.5194/gmd-2020-258
Preprint. Discussion started: 22 September 2020

Geoscientific Model Development Discussions
Open Access

General rules distinguishing primary and secondary stands within the age-class context stem from the Land Use Harmonization dataset version 2 (LUHv2; Hurtt et al. 2017) and with the following modifications: (1a) the primary grid-cell fraction only decreases in size and never gets mixed with existing secondary forests or with abandoned managed land. Only fire creates young age-classes on primary lands. (2a) secondary grid-cell fractions can be mixed with other secondary forest fractions, recently abandoned land, fractions with wood harvest, and recently burned area. General priority rules for deforestation and wood harvest: (1b) For simplicity, deforestation always occurs in the ranking of oldest to youngest age-class, proceeding to deforest each age-class until the prescribed fractional area of deforestation is met. This rule is a conservative estimate of fluxes from deforestation, typically resulting in greater land-to-atmosphere fluxes than if rules were employed that allowed younger age-classes to be preferentially deforested. (2b) wood harvest also occurs in the ranking of oldest to youngest age-class until two conditions are met. Timber harvest occurs on each age-class until a prescribed harvest mass or harvest area is met.

Treatment of immediate emissions and residues: Deforestation results in 100% of heartwood biomass and 50% of sapwood biomass being stored for delay emission in product pools; root biomass is entirely part of belowground litter pools, while 100% leaf and 50% of sapwood biomass becomes part of aboveground litter pools. Grid-cell fractions that underwent land-use change were not mixed with existing managed lands or secondary fractions until all land-use transitions had occurred. This avoids a computational sequence that results in a lower flux if deforestation and abandonment occur in the same year. For wood harvest, 100% of leaf biomass and 40% of the sapwood and heartwood enters the aboveground litter pools, and 100% of root biomass the belowground litter pools; 60% of sapwood and heartwood are assumed to go into a product pool for delayed emission.

Timber from deforestation and harvest in product pools for delayed emission (Earles et al. 2012): For deforestation, 60% of exported wood (i.e., not in litter) goes into a 2-yr product pool and 40% goes into a 25-yr product pool, following the 40:60 efficiency assumption from McGuire et al. (2001). For wood harvest, the model uses space-time explicit data on harvest fractions going into roundwood, fuelwood and biofuel product pools; dataset described further in Sect. *2.3.3*. We use three product pools and assume that 100% of the fuelwood and biofuel fraction goes into the 1-year product pool (emitted in the same year of wood harvest), 50% of the roundwood fraction goes into the 10-year product pool (emitted at rate 10% per year) and the remaining 50% of the roundwood fraction goes into the 100-year product pool (emitted at rate 1% per year).

2.3 Experimental Design and Analysis

2.3.1 Model inputs

Inputs to the model are gridded soil texture (sand, silt, clay fractions) from the USDA Harmonized World Soils Dataset v1.2 (Nachtergaele et al. 2008), annually-varying global-mean [CO_2] (time series available in supplement), and monthly-varying air temperature, precipitation, precipitation frequency, and radiation from the Climate Research Unit (CRU, version TS3.26) data for 1901-2016. Land use, land use change, and wood harvest was prescribed annu-

https://doi.org/10.5194/gmd-2020-258
Preprint. Discussion started: 22 September 2020

ally based on the Land Use Harmonization dataset version 2 (LUHv2; Hurtt et al. 2017), which is used as forcing land-use for the 6th Coupled Model Intercomparison Project (CMIP6; Eyring et al. 2016). The dataset includes fractional area of bi-directional (gross) land use transitions between forested and managed lands, as well as the total biomass of wood harvest on a specified fractional area logged. In this version of LPJ, managed lands (crops, pastures) are treated as grasslands with no irrigation, no fire, and tree PFTs were not allowed to establish. Model representation of land management is an oversimplification to focus on effects of wood harvest.

2.3.2 Qualitative evaluation of simulated stand structure against U.S. Forest Inventory Analysis (FIA) data

U.S. Forest Inventory and Analysis (FIA) – The FIA dataset is freely available at the FIA DataMart web portal (FIADB version 1.6.0.0.2), accessed 2 February 2016. We extracted variables that capture two main axes of structural change as a function of forest age: stem density and tree height. Spatial coordinates of sample plots are 'fuzzed' with imposed error for privacy reasons (FIA User Guide v 6.02; O'Connell et al. 2015). For purposes of this analysis, plot data were aggregated to the spatial scale of U.S. Forest Service *Divisions* (delineated by regional-scale precipitation levels and patterns as well as temperature) minimizing co-location concerns between model-observation comparisons. We filtered the FIA data based on the following criteria. We only included plots that used the national standard plot design (DESIGNCD=1) and were located on forested land (COND_STATUS=1) with no history of major disturbance, stocking, or logging (DSTRBCD=0, TRTCD1=0). We also only included plots that had both sub-plot (168 m^2) samples of live (STATUSCD=1) tree ($\geq$ 5.0 inches diameter) stem density and also micro-plot (13.5 m^2) samples of seedling/sapling (1 to 5 inches diameter) stem density, and where the sub-plot sampling design was the national standard (Tree Table SUBP = [1,4]); LPJ-wsl implicitly includes sapling and adult trees in estimates of tree height and stem density. We assumed that the filtered plots were representative of the true density and distribution of tree species for the general vicinity of the plots and of the USFS Division. Although these requirements for selecting FIA plots reduce the total amount of data, we aimed to make evaluations in a fair manner, in both spatial scale and meaning.

2.3.3 Examining age dynamics: regional simulation for assessing changes in stand structure and ecosystem function

The objectives of the regional simulations were to evaluate demographic patterns of stand structure and function when simulating age-classes using different age-width binning. Two ideal simulations were conducted at a regional scale to sample simulated annual stem density, average tree height, and NEP. The first simulation used the *unequal-bin* age-width setup, $\mathbf{S_{unequalbin}}$, and another used the *10-yr-equalbin* age-width setup, $\mathbf{S_{10yrbin}}$ (Table 2). For both simulations, Fire and LUCLM were not simulated. Instead, 5% of the fractional area of age-classes > 25 years were cleared of biomass annually; the fractional area cleared was re-classified and merged with the youngest age-class. The intent of the setup was to ensure that each grid-cell maintained patches in every age-class for each year of the simulation and avoided situations in which age-classes were only present in 'bad years', or when growing conditions were poor. Both simulations were conducted with a 1000-yr 'spinup' using fixed CO_2 (287 ppm, 'pre-industrial' values) and climate randomly sampled from 1901-1920 to ensure that age distributions were developed and state variables were in dynamic equilibrium (i.e., no trend). A transient simulation then used time-varying CO_2 and climate, as prescribed by model inputs. Stand structure data were analyzed for 1980-2016.

The idealized simulations were performed for the mixed deciduous and evergreen forests of Michigan, Minnesota and Wisconsin, U.S.A (bounding box defined by left: 97.00º W; right: 82.50º W, top: 49.50º N, bottom: 42.00º W). These forests are of moderate temperate climates, with total annual rainfall 815.0 mm/yr (average over 1980-2016, based on CRU TS3.26) with monthly minimum 21.0 mm/mo and maximums of 148.5 mm/mo. Mean annual temperature (1980-2016, CRU TS3.26) was 5.98º C with monthly minimum of –11.45º C and maximum 20.98º C.

Data were pooled for the region over the time period and by age-class. Date were plotted in box plots to show median value, interquartile range and outliers. No attempt was made to de-trend data because there was enough between age-class variation to evaluate general demographic patterns visually.

2.3.4 Examining resilience: idealized simulation of a single event of deforestation, abandonment, regrowth

The objective of the idealized simulation was to evaluate the effect of age-classes on relaxation times following a single deforestation, abandonment and regrowth event within a single grid-cell (Table 2). The relaxation time is defined as the time required for a variable to recover to previous state and is a direct measure of ecosystem resilience (*sensu* Pimm 1984). Two simulations were conducted, the first simulation used the *10-yr-equalbin* age-width setup, $\mathbf{S_{age\_event}}$, and another did not simulate age-classes, $\mathbf{S_{noage\_event}}$ (Table 2). Both simulations were conducted with a 1000-yr 'spinup' using fixed CO_2 (287 ppm, pre-industrial value) and climate randomly sampled from 1901-1920 to ensure that state variables were in dynamic equilibrium. A transient simulation then used time-varying CO_2 and climate, as prescribed by model inputs. Fire and LUCLM were not simulated. Instead, 25% of the fractional area was deforested in year 1910 of the simulation and classified as managed land. Deforestation rules were equally applied for both simulations as described in *Section 2.2.2*. In the following year (1911), the managed land fraction was abandoned and allowed to regrow. The following state variables were plotted over time and visually evaluated: NBP, NEP, NPP, Rh, carbon in biomass.

The idealized simulations were performed for a single grid-cell in a mixed broadleaf and evergreen needleleaf forest in British Columbia, CAN (121.25º W 57.25º N). The grid-cell is a boreal climate with total annual rainfall 473.7 mm/yr (average over 1980-2016, based on CRU TS3.26) with monthly minimum 9.11 mm/mo and maximums of 105.8 mm/mo. Mean annual temperature (1980-2016, CRU TS3.26) was 0.59º C with monthly minimum of –16.9º C and maximum 14.7º C.

2.3.5 Global simulation objectives and setup

There were three main objectives for global simulations. The first objective was to evaluate the contribution of age-class information to global stocks and fluxes. Here, a simulation with age-classes ($\mathbf{S_{age}}$) was compared to a simulation without age-class representation ($\mathbf{S_{noage}}$) (Table 2). The second objective was to determine the relative influence

https://doi.org/10.5194/gmd-2020-258
Preprint. Discussion started: 22 September 2020

Geoscientific Model Development Discussions

of fire and LUCLM on the spatial and temporal distribution of ecosystem ages. For this objective, a Fire-only simulation ($\mathbf{S_{Fire}}$) only had age-classes created by fire, whereas a LUCLM-only simulation ($\mathbf{S_{LU}}$) had age-classes only created by abandonment of managed land or by wood harvest (Table 2). A simulation with both Fire and LUCLM ($\mathbf{S_{FireLU}}$) was used as the baseline for comparison against $\mathbf{S_{Fire}}$ and $\mathbf{S_{LU}}$. The third objective used data from $\mathbf{S_{age}}$ to identify the relative influence of demography versus climate on simulated fluxes (NEP, NPP, and Rh).

For all three simulations, a spinup simulation was run for 1000 years using randomly sampled climate conditions from 1901-1920 and atmospheric CO_2 fixed at pre-industrial levels (287 ppm); spinup ensured that age distributions were initialized under natural conditions and state variables were in dynamic equilibrium (i.e., no trend). A second 'land-use-spinup' procedure was run for 398 years to initialize land use at values for year 1860, resampling climate and fixing CO_2 as in the first spinup. After spinup procedures, climate and CO_2 were allowed to vary until simulation year 2016; in $\mathbf{S_{LU}}$ and $\mathbf{S_{FireLU}}$, land use change and wood harvest varied annually as prescribed by the LUHv2 dataset.

In the first objective (as above), global values for stocks and fluxes include both natural and managed lands. These global estimates conform to typical presentation of global values (Le Quéré et al. 2018), in Petagrams (10^{15}) of carbon. Comparisons are made among simulation types and to values from the literature.

For the second objective, a time series of zonal mean ecosystem ages were analyzed to determine the relative importance of $\mathbf{S_{Fire}}$ and $\mathbf{S_{LU}}$ on the observed distributions in $\mathbf{S_{FireLU}}$. The first assessment was made by visual inspection of zonally-averaged time-series (i.e., Hovmöller plots) for the entire period of transient simulation, years 1860-2016. In addition, for each of $\mathbf{S_{Fire}}$ and $\mathbf{S_{FireLU}}$, a simple linear regression model (age = $\beta_0 + \beta_1$*year, setting 1860 as the reference year and defined as 1) was applied to identify trends in ecosystem age by the following zonal bands: boreal (50° N to 90° N), temperate (23° N to 50° N), and tropics (23° S to 23° N). Trends in LUCLM are, by definition, prescribed *a priori* by the forcing data, but age distributions are not prescribed by inputs per se; instead, the age module is a necessary model structure that allows full realization of the effect of forcing data on age distributions. By contrast, fire is a fully simulated process that integrates feedbacks from climate conditions and fuel loads.

2.3.6 Statistical model to assess relative importance of demography and climate

For the third objective of global simulations – to reduce dimensionality of the data and to assess the relative influence of demography and climate on simulated fluxes – annual flux data from $\mathbf{S_{age}}$ (Table 2) were analyzed from 2000-2016 using generalized linear regression model,

$$flux_{i,yr} = B1_i \times \text{total\_precipitation}_{i,yr} + B2_i \times \text{mean\_temperature}_{i,yr} + B3_{i,age} \times ageclass_{i,yr,age} \tag{6}$$

, where *flux* was one of {NEP, NPP, Rh} in kg C m^{-2} yr^{-1}, precipitation (mm) and temperature (Celsius) data from CRU TS3.26, and age-class was categorical, defined by the age-class code (Table 1), and the beta coefficients (*B*) for subscripts of grid-cells (*i*), years (*yr*) and age-class (*age*). The beta coefficients are therefore unique to every

https://doi.org/10.5194/gmd-2020-258
Preprint. Discussion started: 22 September 2020

Geoscientific Model Development Discussions

grid-cell, and the betas for age-classes are estimated separately for each age-class within the grid-cell ($B3_{i,age}$). An initial test of the model attempted to estimate globally-consistent predictor effects, but the model was found to be a poor fit (*not shown*) and it was assumed that there was too much variation among grid-cells to detect globally-consistent effects. Instead of adding additional gridded fields of predictor variables to account for grid-cell-level variation, the same statistical model was applied and analyzed per-grid-cell. This allowed coefficients of precipitation, temperature and age-class to vary by grid-cell, in essence, reducing the effect of variation in PFT composition, soil texture and hydrology that might otherwise reduce predictive power.

In all per-grid-cell analyses, the intercept term was intentionally omitted from the data model by adding a '-1' term to the data model. The Age-class term in the statistical model ($B3_{i,age}$), as a categorical variable, effectively takes the place of the intercept term anyhow, so the outcome is that estimates are for the absolute effect of each age-class on the predicted flux as opposed to estimates that were relative to the first age-class; this had no impact on estimated coefficients but it did simplify analyses. In grid-cells where only a single age-class was present, the statistical model was defined as ($flux_{i,yr} = B1_i$ total_precipitation$_{i,yr}$ + $B2_i$ mean_temperature$_{i,yr}$ + $B3_i$), leaving the intercept term, in this case – $B3_i$, to be estimated from the data and then re-classifying the intercept term by the age-class code for the grid-cell.

The degrees of freedom (d.f.) of a model for a grid-cell with a single age-class was d.f.=14, based on 17 annual data points to estimate coefficients of three predictors. The degrees of freedom for a grid-cell that had a maximum of 12 age-classes was d.f.=190, based on 204 annual data points to estimate coefficients for 14 predictors. Because the analysis produced statistical results for every grid-cell, the degrees of freedom are not presented elsewhere. Coefficients were only analyzed or mapped when significant at p=0.05.

3 Results

3.1 Model Stand Structure – comparison against inventory data

FIA data were not equally available for every age class, nor for every Division (Figure SM2), but there were enough inventory data across 8 Divisions, spanning subtropical to temperate steppe climates, to qualitatively suggest that LPJ-wsl does capture the expected age-structure patterns in the different climates evaluated. There was a tendency to overestimate stem density in younger age-classes and systematically underestimate tree heights among age-classes (e.g., Figure SM3, Figure SM5), for which the greater number of small individuals could cause the average tree heights to be dampened. However, LPJ-wsl is a big-leaf, single-canopy model and it does not represent multiple pft cohorts in a stand, or more simply, it does not represent vertical heterogeneity. As such, and under the current model architecture and associated assumptions, the cause of the mis-match is unclear. Even still, the more general pattern of modeled stem density and tree height tended to track FIA data, with stem density being maximal in the younger age-classes and declining thereafter, whereas tree height patterns increased more linearly before stabilizing (Figure SM6 to SM9).

FIA data had greater variability among age-classes, regardless of Division. It is a reasonable assumption to say that a large part of this variability results from successional changes in community composition as FIA protocols specify data be taken on every species; although species-level data are available. It is beyond the scope of this study to disentangle these patterns further, but such information could be used to improve simulated age dynamics if models were to include additional plant functional types for a given Division.

3.2 Model Age Dynamics

3.2.1 Dynamics of stand structure and function – regional simulations

Forest structural characteristics of stem density, height, and NEP followed the expected patterns with age with a few exceptions. In $\mathbf{S_{unequalbin}}$ (Table 2), stem density increased from near zero to maximum in the 21-25 yr age-class, before declining non-linearly (Figure 3). By contrast, the gradual increase in stem density in the first age-class in $\mathbf{S_{10\text{-}yrbin}}$ (Table 1) was not readily apparent because this process, which is evident in $\mathbf{S_{unequalbin}}$, occurs entirely within the youngest 1-10 yr age-class in $\mathbf{S_{10\text{-}yrbin}}$. Both simulation setups approach the same stem densities after age ~25; prior differences are due to binning of age-widths.

For average tree height in $\mathbf{S_{unequalbin}}$, there were large tree heights in the youngest age-class, which results from so-called 'survivor' trees (Figure 3). Not all trees are killed-off when a stand-clearing disturbance occurs in LPJ. Although the stand is 'reset' to the youngest age-class, the survivor trees skew the height distribution until the density of establishing saplings subsequently increases and brings down the average tree height to smaller values. This pattern is more akin to what occurs during natural fires or selective harvesting, which can reduce the overall age of a stand but might not result in a complete removal of all trees. By contrast, the skewed age-height pattern is not apparent in $\mathbf{S_{10\text{-}yrbin}}$ (Figure 3) only because the same process is effectively hidden. Both simulation types approach the same average tree heights after age ~25 (Figure 3).

NEP peaked at age-class 5-6 in $\mathbf{S_{unequalbin}}$, before declining non-linearly to the lowest average value in the oldest age-class (Figure 3). Although the unimodal peak was not apparent in $\mathbf{S_{10\text{-}yrbin}}$, the maximum NEP occurred in the youngest age-class and also declined non-linearly thereafter (Figure 3). The decline in NEP after a maximum at 5-6 years was driven mainly by an increase in Rh due to increases in turnover rather than a larger decline in NPP (Figure 4). The peak in NEP did not coincide with maximum stand density at ~20 years. Instead, model dynamics suggest that the total foliar projective cover of tree canopies reaches near maximum (80-95% cover, *not shown*) at 5-6 years, thereafter plant competition reduces NPP while biomass turnover increases, which together cause the apparent decline in NEP. The time period of canopy closure, at 5-6 years, in LPJ-wsl is probably too early, in part due to advanced regeneration (saplings establish at 1.5 m height) and constant establishment rates. The age-class module demonstrates NEP-age relationships consistent with field-based evidence (Ryan et al. 2004, Turner 2010).

Lastly, an emergent pattern was found in the declining portion of the NEP-age curve and approximately follows the functional form $NEPmax*0.70^{age\text{-}agemax}$, where *NEPmax* is the maximum NEP flux at the initial point of decline, *age* is the age of the stand, and *agemax* is the age of the stand where NEP is maximized. Thus, the non-linear decline in NEP is approximately 30% with increasing age. The functional equation holds between year 5-6 to year 25, after which NEP decreases only by 20% with increasing age and the functional form becomes $NEP_{25yr}*0.80^{age-25}$, where NEP_{25yr} is the NEP at year 25. The functional form of the decline in NEP is consistent among climate regions when simulated data is analyzed separately for all U.S. States (*not shown*). It is unclear whether this emergent pattern is strictly the result of model dynamics around canopy closure or if the pattern would be apparent in field data.

3.2.2 Time-series evolution of a deforestation, abandonment and regrow event

A single event of deforestation, abandonment and subsequent forest regrowth caused long-lasting effects and unrealistic model behavior when omitting age-class dynamics. In the simulation without age-classes, $\mathbf{S}_{\mathbf{noage\_event}}$ (Table 2), NEP takes ~30 years to recover to values prior the event, whereas the age-class simulation, $\mathbf{S}_{\mathbf{age\_event}}$, takes only 5-6 years to recover (Figure 5) – a 5-fold change in relaxation times. The quick recovery of NEP in $\mathbf{S}_{\mathbf{age\_event}}$ is due partly to the fact that the fraction of the grid-cell (75%) that was *not* deforested maintained its state variables (carbon stocks in vegetation, soil, litter) unchanged from its prior state, which buffered NEP and dampened the effect of the smaller fraction (25% of grid-cell) that was deforested. Age-class dynamics also contributed an elevated NEP (Figure 4) that quickens the recovery at the grid-cell level. In $\mathbf{S}_{\mathbf{age\_event}}$, there is an elevated NEP in the secondary stand that is sustained for more than 30 years following the event.

In $\mathbf{S}_{\mathbf{noage\_event}}$, vegetation dynamics cause turnover to increase and causes an elevated Rh that is consistently higher than NPP for 30 years after the event. This pattern is striking because NPP recovers quicker than in $\mathbf{S}_{\mathbf{age\_event}}$ and maintains an elevated value for ~30 years. Following a disturbance even in LPJ, stem density and foliar projective cover is reduced but the state variables (carbon in plant organ pools of leaf, stem, root) maintain prior values; this is the reason NPP recovers quickly in the standard-no-age simulation. As stand density increases again, canopy closure initiates competitive dynamics that result in mortality of individuals of the plant population that are generally larger than if the stand had progressed from small to large individuals (as in $\mathbf{S}_{\mathbf{age\_event}}$). The VTFT age-class module also uses the mean-individual approximation, but these unrealistic model dynamics are effectively dampened because stand dynamics are always allowed to occur in natural progression and the relatively small age-widths (10-years) ensure that stand age dynamics (NEP-age trajectories in Figures 3 and 4) most evident in the first 50 years are discretely modeled.

3.3 Global Stocks, Fluxes, and Age Distribution

3.3.1 Stocks and fluxes – $\mathbf{S}_{\mathbf{noage}}$ versus $\mathbf{S}_{\mathbf{FireLU}}$ and convergence in global NEP.

Carbon stocks in biomass are lower in $\mathbf{S}_{\mathbf{age}}$ than in $\mathbf{S}_{\mathbf{noage}}$ by ~40 Pg C globally (Figure 6). Lower global biomass in $\mathbf{S}_{\mathbf{age}}$ can be explained by feedbacks from LUC and Fire that create younger age-classes that have lower overall biomass than in older stands. In addition, age dynamics cause turnover to increase (as in Figures 3 and 4), causing soil carbon to be greater by ~35 Pg C and litter carbon to be greater by 5 Pg C. Taken together, age-class dynamics cause 40 Pg C to be re-allocated from the living biomass pool to the soil-detrital pool, which compounds to alter the mag-

https://doi.org/10.5194/gmd-2020-258
Preprint. Discussion started: 22 September 2020

Geoscientific Model Development
Discussions
Open Access

nitude of fluxes from heterotrophic respiration. Demographic changes in turnover, such as these, are already known to be a large source of uncertainty among projections by global ecosystem models (Friend et al. 2014). What these numbers emphasize, however, is that uncertainty among models could be reduced by explicitly modeling age dynamics.

Net Ecosystem Exchange (NEE; positive fluxes to atmosphere) is only marginally different between $\mathbf{S_{noage}}$ and $\mathbf{S_{age}}$ simulations (mean difference of 0.25 Pg C yr^{-1} over 2000-2010). Compensatory fluxes in Fire and Rh explain the small difference in NEE at global scales. Fire fluxes in $\mathbf{S_{age}}$ are lower by 0.92 Pg C yr^{-1} in the 2000s than in the $\mathbf{S_{noage}}$, but fluxes from Rh are greater in $\mathbf{S_{age}}$ by 1.61 Pg C yr^{-1} and NPP also greater by 0.55 Pg C yr^{-1}. The fluxes in Fire, Rh and NPP largely offset to minimize differences in NEE from age dynamics.

The question still remains – should there be an expectation for greater differences in NEE (?), perhaps not. Consider that deforestation (areal changes prescribed the same in $\mathbf{S_{noage}}$ and $\mathbf{S_{age}}$) occurs from the oldest to youngest age-class in $\mathbf{S_{age}}$, following greater to lower overall biomass, respectively. The deforestation flux is greater in the $\mathbf{S_{age}}$ by only 0.04 Pg C yr^{-1} in 2000s compared to deforestation fluxes in $\mathbf{S_{nosge}}$, which makes sense given that low-biomass age-classes are not preferentially deforested or harvested. By contrast, fire is not prescribed in LPJ-wsl but it is simulated based on soil moisture and a minimum fuel load. It is not clear outright how age-dynamics affect soil moisture, but fluxes from fire would need to be proportional to the biomass in a patch. By definition in $\mathbf{S_{age}}$, there is explicit representation of lower-biomass patches (younger age-classes) than in $\mathbf{S_{noage}}$, and a series of fires or disturbances within the grid-cell would drive the age distribution towards younger states, exacerbating differences in downstream fluxes as well. That global NEE only changed marginally when simulating global age dynamics was a surprise, but explained by shifts in the carbon pools and compensatory fluxes, then the patterns appear to make sense. In light of these compensation effects, however, there is a great need to benchmark fluxes from critical feedbacks, particularly from fire in this case. It is beyond the scope of this paper to do so, and best available datasets, such as the Global Fire Emission Database (GFEDv4s; van der Werf et al. 2017) do not lend themselves to direct comparison with fire fluxes from LPJ. GFED includes fires from deforestation and land management that are tracked differently in LPJ-wsl – as a land use change flux, which cannot simply be added to the fire flux for direct comparison to GFED without double counting. In any manner, this issue is stated as a suggestion for future development and refinement.

3.3.2 Global age-class distribution – contribution of fire and LUCLM to age distributions

Average ecosystem age, generated by the model, differed greatly among continents (Figure 7), with large areas of old-growth forests in Asia, Europe, North and South America skewing the distribution towards older ages. The largest area of young ecosystems was located in Africa and Australia (Figure 1), wherein age-classes comprised an ~1:1 age to fractional area ratio of vegetated land (age-classes < 20 years comprise ~20% of the vegetated land area in Africa and Australia and age-classes < 40 years ~ 40% of vegetated land area; Figure 7).

The primary driver of zonal age distributions was Fire (Figure 8), which was responsible for a ~23 yr difference in

https://doi.org/10.5194/gmd-2020-258
Preprint. Discussion started: 22 September 2020

zonal ages (Table 3). There was a significant decrease in zonal ecosystem age over time due to fire (Table 3), most likely from feedbacks due to enhanced fuel (biomass) production from CO_2 fertilization. The causes were not explored further because feedbacks between fire-climate-CO_2 are largely constrained by the fire module itself. A proper attribution to trends in fire is better suited to fire model inter-comparisons ('FireMIP' *in* Hanston et al. 2016). The emphasis here is simply that fire was a major driver of age distributions and fire-age relationships had an apparent trend over time. Between simulation years 1860 and 2016, fire caused a total change in ecosystem age, integrated over the time period, by -1.5 years in boreal zones (negative values for a decrease in age), whereas the change was greater in temperate (-6.7 years) and tropical (-8.24 years) zonal bands (Table 3). The larger trend in temperate and tropical latitudes might be due to increasing warming temperatures in contemporary times, causing dryer conditions more suitable for fire, or from increases in fuel loads from CO_2 fertilization. A more convincing argument would require support from additional factorial experiments to identify to the casual driver of the trend differences.

After accounting for the effects of fire, LUCLM caused a much greater change over time in the zonal ecosystem age (Figure 9). Integrating from 1860 to 2016, LUCLM caused a zonal change in ecosystem age by -6.1 years in boreal zones, whereas the change in ecosystem age from LUCLM in temperate and tropical zones was -21.6 years, with no significant difference in the trend due to LUCLM among these zonal bands (Table 3). These patterns are consistent with the concentration of deforestation in the tropics and land use change in temperate latitudes, as described by the forcing data (Hurtt et al. 2011, Hurtt et al. 2017).

3.4 Global Demographic Effects on NPP and Rh

3.4.1 Simplification of LPJ-wsl via a statistical model

The statistical model (flux = $B1$ precipitation + $B2$ temperature + $B3_{age}$ age-class; *See Sect. 2.3.6* for details) had great predictive power for NPP and Rh, with R^2 between 0.95-0.98 (Figure 10). The predicted fluxes were at annual time scales, with annual variation being mainly driven by total annual precipitation and mean annual temperature, whereas the mean state (intercept) being predicted by the age-class. The predictive power for a model of NEP was slightly worse (R^2 between 0.60-0.65; SM Figure 1). The effect of precipitation, temperature and age-class on NEP was not consistent enough for robust predictions, but more specifically, the predictors had different effects on NPP versus Rh leading to poorer model fit. As it is, NEP is better derived as predictions of NPP minus predictions of Rh rather than having a standalone model for NEP.

3.4.2 *The Effective Range of Predictors – assessing relative importance of demography on predicted fluxes*

The "Effective Range of the Predictors" were mapped to visualize spatial patterns of the range of effects, given observed values for the predictors (Figure 11). In essence, the effective range of the predictor is a measure of the dynamic range in the predicted flux due to changes in precipitation, temperature or demography. It is calculated as the grid-cell-specific beta coefficient multiplied by the observed range of the predictor for a given grid-cell, which helps constrain the effect of the predictor on the predicted flux to realistic values. For example, for the LPJ-wsl grid-cell at

https://doi.org/10.5194/gmd-2020-258
Preprint. Discussion started: 22 September 2020

location [110.75 W 50.25 N], the ß estimate for the effect of precipitation on NPP was 0.0028, and the range of observed precipitation (based on CRU TS36) was 282 mm, then the effective range of the predictor on the flux was calculated as 0.0028*282 = 0.79 kg C m^{-2} yr^{-1}.

The effect of precipitation on NPP was clearly greater in the central USA and Eastern Australia (range of effect ~ 0.70 kg C m^{-2} yr^{-1} due to precipitation) than in other locations, and overall, precipitation had a stronger (positive) effect on NPP than on Rh (Figure 11). It was also clear from the maps that the direction of the effect of temperature on NPP was more spatially varied in the direction of effect (both positive and negative) than other predictors (Figure 11). The effects of precipitation and temperature displayed similar spatial patterns in both primary and secondary stands, which was a good indicator that the model was performing as expected because, within the LPJ-wsl model, the distinction between primary and secondary stands is mainly to track land use histories and there was no reason, *a priori*, that climate effects should differ substantially between the two stand types.

The effective range of demography on fluxes was generally lower than the effective range of precipitation and temperature, but there were regions where the range of demographic effects were just as important as, or greater than, the climate predictors. The demographic effect on NPP ranged between 0.30-0.60 kg C m^{-2} yr^{-1} in Eastern North America, Western Europe, Central Africa, Eastern China, Tropical Asia, and distributed smaller areas of South America (Figure 11), whereas it was at maximum ~0.10 kg C m^{-2} yr^{-1} in other regions. The higher demographic effect was predominately on secondary stands (Figure 12), but there was also a distinct absence of primary stands in these same areas (Figure 11) so it could not be said definitively if the higher demographic effect was due to a wider age distribution, and therefore a greater demographic effect, or simply due to the productivity of these locations.

3.4.3 Frequency distribution of demographic effects

The global mean demographic effect on NPP on primary stands was 0.078 ± 0.063 [0, 1.37] kg C m^{-2} yr^{-1} (μ ± stdev. [min, max]), whereas on secondary stands it was 0.160 ± 0.141 [0, 1.33] kg C m^{-2} yr^{-1}. There were differences in the spatial distribution of primary and secondary stands that led to the disparity in global mean values of the demographic effect. On primary stands, the distribution of age-classes with maximum NPP flux was skewed towards the second (11-20 years) age-class having the maximum NPP flux, whereas on secondary stands, the maximum NPP flux was in the first (1-10 years) and also in the second age-class (Figure 12). The first class was categorized as 1-10 years, but in the presence of constant renewal, an age-class can effectively be younger than an equivalent age-class without such recurrent disturbance. Furthermore, on primary stands, fire is the only mechanism that creates young age-classes, whereas land management also creates young age-classes on secondary stands. It is possible for wood harvest, a form of simulated land management, to result in advanced regeneration of younger stands if harvest demand is met without 'clear-cutting' the prescribed fractional area under harvest. Currently, the model structure does not lend itself to say definitively the cause of the difference in the age-class of maximum flux, but the only process that differs between primary and secondary stands is land management, so it is reasonable to assume that land management is the cause of the difference. In any manner, global values for age-effects for NPP on primary and secondary stands were also skewed towards greater values on secondary stands, but more due to the absence of primary stands in productive areas where secondary stands dominated (e.g., Eastern U.S.A.).

Following a similar pattern, the demographic effects on Rh were greater on secondary stands than on primary stands (Figures 11 and 12), which could be partly explained by the differential coverage of secondary and primary stands, but also by historical land use. LUCLM leads to overall greater inputs to soil and litter carbon pools than does fire, and the latter is simulated in the same manner on secondary stands as on primary stands. In LPJ, wood harvest is only 60% efficient, leaving dead biomass 'residue' as a legacy flux. An increase of carbon in the litter and soil pools would add additional mass that can be respired during heterotrophic respiration, and which manifests as a larger demographic effect on Rh, ranging from 0.25 to 0.70 kg C m^{-2} yr^{-1} on the high-end (Figure 12).

4 Discussion

4.1 Distribution of Ecosystem Age on Earth

The LPJ-wsl age-module simulates the upper limit of age-class distributions on Earth (Figure 13) and captures important demographics effects on NPP and Rh. Simulations demonstrate that fire and LUCLM have been driving the latitudinal age distribution towards younger states in contemporary times (Figure 8), suggesting an increasing role of age dynamics on global ecosystem functioning. Whereas time is the only mechanism that increases ecosystem age, any additional disturbance not explicitly modeled in this study will decrease age.

The simulations omit widespread disturbances of windstorms, flood, pest and disease outbreak, selective logging, and other processes that would modify stand structure and function. For instance, small-scale logging activity is a dominant disturbance in South Eastern U.S.A. (Williams et al. 2016) but it is underestimated by the LUCLM driver data in this study ('LUHv2', Hurtt et al. 2017); otherwise the simulated age of secondary forests in this region (~100 years) would be lower and closer to inventory-based age estimates of these forests (< 50 years; *Figure 4 in* Pan et al. 2011b). Furthermore, the fire module has been well evaluated at global scale (Thonicke et al. 2001) but it is overly simplistic (Hantson et al. 2016), so it is more likely that effects of fire are much greater than simulated in this study. It is clear then that this study underestimates disturbances rather than overestimates them, and as such, these simulations overestimate ecosystem age. But again, additional disturbances would only lead to younger age-classes, enhancing the role of age dynamics in regional and global carbon cycles.

Even with these caveats in mind, the findings presented retain utility as insight into the way age-class dynamics integrate into our broader understanding of global carbon dynamics. Ecosystem demographics likely play a larger role than suggested here, and on regional scales, demographic effects on NPP and Rh are already identified by this study as more important in East Asia, Tropical Asia, Europe, Central Africa, Eastern North America, and Tropical South America than they are in other regions, where average ecosystem ages are much older.

4.2 Age Dynamics Increase Turnover

Geoscientific Model Development Discussions

In an analysis by Friend et al. (2014), it was determined that demographic processes (age-dependent mortality and turnover) influence carbon residence time (1/Turnover), which was found to be a major source of uncertainty in future projections by global ecosystem models. In this study, it was demonstrated that simulation of age-classes led to a ~40 Pg C shift from live vegetation to the soil-litter pool, effectively an increase in biomass turnover. Further, relaxation times, or the time to return to a previous state, were up to 30 years in the no-age simulation (**S_{noage_event}**; Figure 5) but relaxation times were less than 10 years when simulating age-classes, suggesting that uncertainty in carbon residence time can be reduced by improving representation of demographics in models. Omitting age-class representation in models can leave long-lasting patterns in simulated fluxes that could inflate land use change fluxes at global scales when considering legacy fluxes from past land use change (Pongratz et al. 2014). The current state of knowledge is that fluxes from gross land use change and land management cause greater-than-expected land use fluxes (Arneth et al. 2017), but existing models that estimate the global land use flux (Arneth et al. 2017, Le Quéré et al. 2018) do not include age dynamics. If resiliency is inversely proportional to relaxation times (a quicker return to previous states is represented by shorter relaxation times, therefore greater resiliency; Pimm 1984, Tilman and Downing 1994), then instead of land use change fluxes being 'greater than assumed' (Arneth et al. 2017), we might rethink the land as being 'more resilient than expected' when demographic effects are considered at large scales.

4.3 Forecasting Demographic Effects with a Simplified Statistical Model

The modeling community has made increasing effort to simplify complex models using a traceability framework (Friedlingstein et al. 2006, Xia et al. 2013). Statistical emulators, from matrix models (Huang et al. 2018) to accounting-type statistical models, which track individual carbon pools (Xia et al. 2013, Ahlström et al. 2015), have been developed to reduce the dimensionality of simulated state variables. However, statistical modeling by linear regression can be a more straightforward approach, as long as the statistical model shows promise.

We found that LPJ-wsl fluxes of NPP and Rh could be predicted at annual timescales by three terms, precipitation, temperature and age-class. Part of the success of the data model came from allowing coefficients to vary by grid-cell. This allowed the intercept (age-class) term to effectively capture grid-cell level variation in soil texture (which influences soil hydrology and plant available water), PFT composition and cloud cover. Another insight was that climate and age-class had differential effects on NPP versus Rh, which makes sense and ultimately led to poorer fit of the NEP model (NEP = NPP – Rh). It might have been possible to improve upon the NPP model further by separately modeling GPP and Autotrophic Respiration (NPP = GPP – Ra) because climate might also have differential effects on GPP than on Ra, but suffice to say that the NPP statistical model was robust.

Although unexplored in this study, the spatial datasets of predictor coefficients could be used within an emulator (Xia et al. 2013, Ahlström et al. 2015) to forecast NPP and Rh, while exploring extreme climate scenarios (Reichstein et al. 2013), such as drought. Such application would allow for a much quicker exploration of scenarios and could include a more explicit treatment of uncertainty that would otherwise be too costly for the simulation model in terms of computing time. The spatial dataset of precipitation coefficients has an equivalent meaning to spatial maps of climatic sensitivity. In fact, the maps of the effective range of precipitation on NPP (Figure 11) show areas where the precipitation effect is largest, notably in semi-arid biomes – a biome that is known to be highly sensitive to precipitation and has been shown to play an important role in the inter-annual variability of global-scale fluxes (Poulter et al. 2014, Ahlström et al. 2015). But what if, in a given year, semi-arid biomes received their maximum annual precipitation, while every other biome received its lowest annual precipitation – can anomalously high annual precipitation and high productivity events in some regions overcome anomalously low precipitation and low productivity events in other regions? This type of question is best suited for exploration within a simplified statistical model that maintains fidelity to the process-based model because effects of climate on fluxes can be explored quicker, easier, and with a better treatment of statistical uncertainty.

4.2 Vector Tracking of Fractional Transitions (VTFT) – modeling age-classes in global models

The VTFT approach simulated classic demographic responses in NPP and Rh (Figure 4), a differential in younger age-classes that led to a larger carbon sink in the youngest stands. These demographic responses are inherent within the original formulation in LPJ; that is, establishment rates and the process of self-thinning of stand density over time as plants grow and compete (for space, light, water resources) have been unchanged. In the original formulation of LPJ-wsl (prior to this study), and under a hypothetical scenario where a disturbance clears the biomass from the entire grid-cell (0.5° ~ 2,500 km^2), the resultant evolution of stand structure and fluxes would produce the same pattern as in the age-module, such as the age-NPP pattern from Figure 4. It is often the case, however, that smaller disturbances (<< 2,500 km^2) occur regularly as opposed to a much larger disturbance the size of the entire grid-cell. As such, in the original formulation of LPJ, the potential benefits of demographic responses are often masked (as demonstrated in *Section 3.2.2*; Figure 5). One can then say that the VTFT age-module reveals intrinsic demographic responses and model behavior that would rarely emerge otherwise.

Total runtime for global age-class simulations ($\mathbf{S_{age}}$) was ~8 hrs on 32 Intel Xeon CPUs, including spinup to transient simulations, whereas the total runtime for the no-age simulations ($\mathbf{S_{noage}}$) was ~3 hrs. On a limited sample of single grid-cell simulations, there was a 4- to 6-fold increase in runtimes, but not all grid-cells require simultaneous tracking of every age-class so the increase in runtime of global simulations was lower than expected from per-grid-cell estimates.

4.3 Opportunities for Improving Modelled Age-dynamics

There a number of opportunities for refining the age-module. Incorporating additional disturbances within the model, which will help simulate age distributions more consistent with inventory (Pan et al. 2011a) and satellite (Pugh et al. 2019b) data and contribute to more scientifically relevant questions. Modeled disturbances need not be complex to explore their effects on age distributions, they only need to reset a fractional area to the youngest age-class. For example, windstorms from Hurricanes are known to be a large disturbance of Eastern North American forests (Dale et al. 2001). Data on Hurricane return intervals and locations of landfall in Eastern North America have been available for some time (Keim et al. 2007), and could be used to prescribe a periodic resetting of age-classes to assess the

https://doi.org/10.5194/gmd-2020-258
Preprint. Discussion started: 22 September 2020

demographic effect of Hurricanes on ecosystem function. In another example, forest gaps represent areas of high production because of high resource abundance relative to the surrounding areas. The distribution of forest gaps also has a predictable power-law relationship with size of the gap (Asner et al. 2013), and this fact lends itself well for representing gaps within the framework of the current age-module.

There are limitations to the current framework of the model, which are more difficult to overcome and will require more effort in model development. In this version of the model, plant composition and competitive dynamics in young age-classes are not representative of early successional dynamics because there is a lack of plant trait variation in the current set of PFTs that could otherwise represent a wider range of growth strategies, turnover, and production (Pütz et al. 2011, Fischer et al. 2016, Miller et al. 2016). There is also no height variation within an age-class, for lack of a radiative transfer model; each age-class in this version of LPJ-wsl is an even-height stand. Demographic patterns in this study (age-NPP, age-Rh, relaxation times by age-class) will inevitably differ when, and if, additional trait and height variation is incorporated into the model.

Recent model developments in JSBACH4 (Nabel et al. 2019) and ED-2.2 (Longo et al. 2019) could point the way forward for incorporating a greater amount of vertical heterogeneity in LPJ-wsl, as well as in other models. In any case, the age-module in LPJ-wsl v2.0 now contributes to an ensemble of global models with demographic capabilities.

5. Code and Data Availability

LPJ-wsl v2.0 model code, in its entirety, is freely available at <https://github.com/benpoulter/LPJ-wsl_v2.0>. Code used for analyses and figure production are available at <https://github.com/lcalle/VTFT_demography>. Associated data necessary to reproduce the analyses and figures, as well as a copy of the analysis code is permanently archived at the Dryad Digital Repository <https://doi.org/10.5061/dryad.k6djh9w4x>.

6. Author Contributions

LC and BP designed the model experiments and LC carried them out. LC developed the code for the age-class module and performed the simulations. LC and BP prepared the manuscript.

7. Acknowledgements

Computational efforts were performed on the Hyalite High Performance Computing System, operated and supported by University Information Technology Research Cyberinfrastructure at Montana State University. LC was supported by a National Aeronautics and Space Administration Earth and Space Science Fellowship (NASA ESSF 2016-2019, Grant# NNX16AP86H). This work contributed to the 3DSI Project (NASA proposal #16-CARBON16-0124). Thanks to Paul Montesano, Bryce Currey, and Tom Pugh for comments on the manuscript.

8. Literature Cited

https://doi.org/10.5194/gmd-2020-258
Preprint. Discussion started: 22 September 2020

Ahlström, A., Xia, J., Arneth, A., Luo, Y., and Smith, B.: Importance of vegetation dynamics for future terrestrial carbon cycling. *Environmental Research Letters*, doi: 10.1088/1748-9326/10/5/054019, 2015.

Ahlström, A., Raupach, M. R., Schurgers, G., Smith, B., Arneth, A., Jung, M., Reichstein, M., Canadell, J. G., Friedlingstein, P., Jain, A. K., Kato, E., Poulter, B., Sitch, S., Stocker, B. D., Viovy, N., Wang, Y. P., Wiltshire, A., Zaehle, S., and Zeng, N.: The dominant role of semi-arid ecosystems in the trend and variability of the land CO_2 sink. *Science*, 348, 895-898, doi: 10.1126/science.aaa1668, 2015.

Arneth, A., Sitch, S., J. Pongratz, Stocker, B. D., Ciais, P., Poulter, B., Bayer, A. D., Bondeau, A., Calle, L., Chini, L. P., Gasser, T., Fader, M., Friedlingstein, P., Kato, E., Li, W., Lindeskog, M., Nabel, J. E. M. S., Pugh, T. A. M., Robertson, E., Viovy, N., Yue, C., and Zaehle, S.: Historical carbon dioxide emissions caused by land-use changes are possibly larger than assumed. *Nature Geoscience*, 10, doi: 10.1038/NGEO2882, 2017.

Asner, G. P., Kellner, J. R., Kennedy-Bowdoin, T., Knapp, D. E., Anderson, C., and Martin, R. E.: Forest canopy gap distributions in the Southern Peruvian Amazon. *PLoS ONE*, 8, e60875, doi:10.1371/journal.pone.0060875, 2013.

Box, E. O.: Plant functional types and climate at the global scale. *Journal of Vegetation Science*, 7, 309-320, 1996.

Earles, J. M., Yeh, S. and Skog, K. E.: Timing of carbon emissions from global forest clearance. *Nature Climate Change*, 2, 682-685, doi:10.1038/NCLIMATE1535, 2012.

Dale, V. H., Joyce, L. A., McNulty, S., Neilson, R. P., Ayres, M. P., Flannigan, M. D., Hanson, P. J., Irland, L. C., Lugo, A. E., Peterson, C. J., Simberloff, D., Swanson, F. J., Stocks, B. J., and Wotton, B. M.: Climate change and forest disturbance. *BioScience*, 51, 723-734, 2001.

Drake, J. E., Raetz, L. M., Davis, S. C., and DeLucia, E. H.: Hydraulic limitation not declining nitrogen availability causes the age-related photosynthetic decline in loblolly pine (*Pinus taeda* L.). *Plant, Cell and Environment*, 33, 1756-1766, doi: 10.1111/j.1365-3040.2010.02180.x, 2010.

Drake, J. E., Davis, S. C., Raetz, L. M., and DeLucia, E. H.: Mechanisms of age-related changes in forest production: the influence of physiological and successional changes. *Global Change Biology*, 17, 1522-1535, doi: 10.1111/j.1365-2486.2010.02342.x, 2011.

Eyring, V., Bony, S., Meehl, G. A., Senior, C. A., Stevens, B., Stouffer, R. J., and Taylor, K. E.: Overview of the Coupled Model Intercomparison Project Phase 6 (CMIP6) experimental design and organization. *Geoscientific Model Development*, 9, 1937-1958, doi: 10.5194/gmd-9-1937-2016, 2016.

FAO-FRA. U.N. Food and Agriculture Organization 2015 Forest Resource Assessment.

Farquhar, G. D., von Caemmerer, S., and Berry, J. A.: A biochemical model of photosynthetic CO_2 assimilation in leaves of C_3 plants. *Planta*, 149, 78-90, 1980.

https://doi.org/10.5194/gmd-2020-258
Preprint. Discussion started: 22 September 2020

Geoscientific Model Development
Discussions

Fischer, R., Bohn, F., de Paula, M. D., Dislich, C., Groeneveld, J., Gutiérrez, A. G., Kazmierczak, M., Knapp, N., Lehmann, S., Paulick, S., Pütz, S., Rödig, E., Taubert, F., Köhler, P., and Huth, A.: Lessons learned from applying a forest gap model to understand ecosystem and carbon dynamics of complex tropical forests. *Ecological Modelling*, 326, 124-133, doi: 10.1016/j.ecolmodel.2015.11.018, 2016.

Friend, A. D., Lucht, W., Rademacher, T. T., Keribin, R., Betts, R., Cadule, P., Ciais, P., Clark, D. B., Dankers, R., Falloon, P. D., Ito, A., Kahana, R., Kleidon, A., Lomas, M. R., Nishina, K., Ostberg, S., Pavlick, R., Peylin, P., Schaphoff, S., Vuichard, N., Warszawski, Wiltshire, A., and Woodward, F. I.: Carbon residence time dominates uncertainty in terrestrial vegetation responses to future climate and atmospheric CO_2. *Proceedings of the National Academy of Sciences of the United States of America*, 111, 3280-3285, doi: 10.1073/pnas.1222477110, 2014.

Friedlingstein, P., Cox, P., Betts, R., Bopp, L., von Bloh, W., Brovkin, V., Cadule, Pl, Doney, S., Eby, M., Fung, I., Bala, G., John, J., Jones, C., Joos, F., Kato, T., Kawamiya, M., Knorr, W., Lindsay, K., Matthews, H. D., Raddatz, T., Rayner, P., Reick, C., Roeckner, E., Schnitzler, K.-G., Schnur, R., Strassmann, K., Weaver, A. J., Yoshikawa, C., and Zeng, N.: Climate-carbon cycle feedback analysis: Results from the C^4MIP Model Intercomparison. *Journal of Climate*, 19, 3337-3353, 2006.

Frolking, S., Palace, M. W., Clark, D. B., Chambers, J. Q., Shugart, H. H., and Hurtt, G. C.: Forest disturbance and recovery: A general review in the context of spaceborne remote sensing of impacts on aboveground biomass and canopy structure. *Journal of Geophysical Research,* 114, G00E02, doi:10.1029/2008JG000911, 2009.

Gitz, V., and Ciais, P.: Amplifying effects of land-use change on future atmospheric CO_2 levels. *Global Biogeochemical Cycles,* 17, 1024, doi:10.1029/2002GB001963, 2003.

Goldewijk, K. K.: Estimating global land use change over the past 300 years: The HYDE Database. *Global Biogeochemical Cycles*, 15, 417-433, 2001.

Hantson, S., Arneth, A., Harrison, S. P., Kelley, D. I., Prentice, I. C., Rabin, S. S., Archibald, S., Mouillot, F., Arnold, S. R., Artaxo, P., Bachelet, D., Ciais, P., Forrest, M., Friedlingstein, P., Hickler, T., Kaplan, J. O., Kloster, S., Knorr, W., Lasslop, G., Li, F., Mangeon, S., Melton, J. R., Meyn, A., Sitch, S., Spessa, A., van der Werf, G. R., Voulgarakis, A., and Yue, C.: The status and challenge of global fire modelling. *Biogeosciences*, 13, 335903375, doi:10.5194/bg-13-3359-2016, 2016.

Haxeltine, A., and Prentice, I. C.: A general model for the light-use efficiency of primary production. *Functional Ecology*, 10, 551-561, 1996.

Haverd, V., Smith, B., Nieradzik, L. P., and Briggs, P. R.: A stand-alone tree demography and landscape structure module for Earth system models: integration with inventory data from temperate and boreal forests. *Biogeosciences*, 11, 4039-4055, doi:10.5194/bg-11-4039-2014, 2014.

Geoscientific Model Development Discussions

Houghton, R. A.: The annual net flux of carbon to the atmosphere from changes in land use 1850-1990. *Tellus B*, 51B, 298-313, 1999.

Huang, Y., Lu, X., Shi, Z., Lawrence, D., Koven, C. D., Xia, J., Du, Z., Kluzek, E., and Luo, Y.: Matrix approach to land carbon cycle modeling: A case study with the Community Land Model. *Global Change Biology*, 24, 1394-1404, doi: 10.1111/gcb.13948, 2018.

Hurtt, G. C., Frolking, S., Fearon, M. G., Moore, B., Shevliakova, E., Malyshev, S., Pacala, S. W., and Houghton, R. A.: The underpinnings of land-use history: three centuries of global gridded land-use transitions, wood-harvest activity, and resulting secondary lands. *Global Change Biology*, 12, 1208-1229, doi: 10.1111/j.1365-2486.2006.01150.x, 2006.

Hurtt, G. C., Chini, L. P., Frolking, S., Betts, R. A., Feddema, J., Fischer, G., Fisk, J. P., Hibbard, K., Houghton, R. A., Janetos, A., Jones, C. D., Kindermann, G., Kinoshita, T., Goldewijk, K. K., Riahi, K., Shevliakova, E., Smith, S., Stehfest, E., Thomson, A., Thornton, P., van Vuuren, D. P., and Wang, Y. P.: Harmonization of land-use scenarios for the period 1500-2100: 600 years of global gridded annual land-use transitions, wood harvest, and resulting secondary lands. *Climatic Change*, 109, 117-161, doi: 10.1007/s10584-011-0153-2, 2011.

Hurtt G, Chini L, Sahajpal R, and Frolking S.: Harmonization of global land-use change and management for the period 850-2100, version 2. Available at luh.umd.edu/data.shtml, 2017.

Keim, B. D., Muller, R. A., and Stone, G. W.: Spatiotemporal patterns and return periods of tropical storm and hurricane strikes from Texas to Maine. *Journal of Climate*, 20, 3498-3509, doi: 10.1175/JCLI4187.1, 2007.

Kondo, M., Ichii, K., Patra, P. K., Poulter, B., Calle, L., Koven, C., Pugh, T. A. M., Kato, E., Harper, A., Zaehle, S., and Wiltshire, A.: Plant regrowth as a driver of recent enhancement of terrestrial CO2 uptake. *Geophysical Research Letters*, 45, 4820-4830, doi: 10.1029/2018GL077633, 2018.

Lawrence, D.M., Fisher, R.A., Koven, C.D., Oleson, K.W., Swenson, S.C., Vertenstein, M., Andre, B., Bonan, G., Ghimire, B., van Kampenhout, L., Kennedy, D., Kluzek, E., Knox, R., Lawrence, P. J., Li, F., Li, H., Lombardozzi, D., Lu, Y., Perket, J., Riley, W.J. Sacks, W.J., Shi, M., Wieder, W.R., Xu, C., Ali, A., Badger, A., Bisht, G., Broxton, P., Brunke, M., Buzan, J., Clark, M., Craig, A., Dahlin, K., Drewniak, B., Fisher, J. B., Flanner, M., Gentine, P., Lenaerts, J., Levis, S., Leung, L. R., Lipscomb, W. H., Pelletier, J. D., T., Ricciuto, D. M., Sanderson, B. M., Shuman, J., Slater, A., Subin, Z., Tang, J., Tawfik, A., Thomas, R. Q., Tilmes, S., Vitt, F., and Zeng, X.: Technical description of version 5.0 of the Community Land Model (CLM). The National Center for Atmospheric Research, 2019.

Le Quéré, C., Andrew, R. M., Friedlingstein, P., Sitch, S., Pongratz, J., Manning, A. C., Korsbakken, J. I., Peters, G. P., Canadell, J. G., Jackson, R. B., Boden, T. A., Tans, P. P., Andrews, O. D., Arora, V. K., Bakker, D. C. E., Barbero, L., Becker, M., Betts, R. A., Bopp, L., Chevallier, F., Chini, L. P., Ciais, P., Cosca, C. E., Cross, J., Currie, K., Gasser, T., Harris, I., Hauck, J., Haverd, V., Houghton, R. A., Hunt, C. W., Hurtt, G. C., Ilyina, T., Jain, A. K., Kato, E., Kautz, M., Keeling, R. F., Goldewijk, K. K., Körtzinger, Landschützer, P., Lefèvre, N., Lenton, A., Lienert, S., Lima, I., Lombardozzi, D., Metzl, N., Millero, F., Monteiro, P. M. S., Munro, D. R., Nabel, J. E. M. S., Nakaoka, S., Nojiri, Y., Padin, X. A., Peregon, A., Pfeil, B., Pierrot, D., Poulter, B., Rehder, G., Reimer, J., Rödenbeck, C., Schwinger, J., Séférian, R., Skjelvan, I., Stocker, B. D., Tian, H., Tilbrook, B., Tubiello, F. N., van der Laan-Luijkx, I. T., van der Werf, G. R., van Heuven, S., Viovy, N., Vuichard, N., Walker, A. P., Watson, A. J., Wiltshire, A. J., Zaehle, S. & Zhu, D.: Global Carbon Budget. *Earth System Science Data*, 10, 405-448, doi: 10.5194/essd-10-405-2018, 2018.

Lindeskog, M., Arneth, A., Bondeau, A., Waha, K., Seaquist, J., Olin, S., and Smith, B.: Implications of accounting for land use in simulations of ecosystem carbon cycling in Africa. *Earth System Dynamics*, 4, 385-407, doi: 10.5194/esd-4-385-2013, 2013.

Longo, M., Knox, R. G., Medvigy, D. M., Levine, N. M., Dietze, M. C., Kim, Y., Swann, A. L. S., Zhang, K., Rollinson, C. R., Bras, R. L., Wofsy, S. C., and Moorcroft, P. R.: The biophysics, ecology, and biogeochemistry of functionally diverse, vertically and horizontally heterogeneous ecosystems: the Ecosystem Demography model, version 2.2 – Part 1: Model description. *Geoscientific Model Development*, 12, 4309-4346, doi: 10.5194/gmd-12-4309-2019, 2019.

McGuire, A. D., Sitch, S., Clein, J. S., Dargaville, R., Esser, G., Foley, J., Heimann, M., Joos, F., Kaplan, J., Kicklighter, D. W., Meier, R. A., Melillo, J. M., Moore III, B., Prentice, I. C., Ramankutty, N., Reichenau, T., Schloss, A., Tian, H., Williams, L. J., and Wittenberg, U.: Carbon balance of the terrestrial biosphere in the twentieth century: Analyses of CO_2, climate and land use effects with four process-based ecosystem models. *Global Biogeochemical Cycles*, 15, 183-206, 2001.

Medvigy, D., Wofsy, S. C., Munger, J. W., Hollinger, D. Y., and Moorcroft, P. R.: Mechanistic scaling of ecosystem function and dynamics in space and time: Ecosystem Demography model version 2. *Journal of Geophysical Research*, 114, G01002, doi:10.1029/2008JG000812, 2009.

Miller, A. D., Dietze, M. C., DeLucia, E. H., and Anderson-Teixeira, K. J.: Alteration of forest succession and carbon cycling under elevated CO_2. *Global Change Biology*, 22, 351-363, doi: 10.1111/gcb.13077, 2016.

Nabel, J. E. M. S., Naudts, K., and Pongratz, J.: Accounting for forest age in the tile-based dynamic global vegetation model JSBACH4 (4.20p7; git feature/forests) – a land surface model for the ICON-ESM. *Geoscientific Model Development*, doi: 10.5194/gmd-2019-68, 2019.

Nachtergaele, F., Van Velthuizen, H., Verelst, L., Batjes, N., Dijkshoorn, K., Van Engelen, V., Fischer, G., Jones, A., Montanarella, L., and Petri, M.: Harmonized world soil database, FAO, Rome, Italy and IIASA, Laxenburg, Austria, 2008.

O'Connell, B. M., LaPoint, E. B., Turner, J. A., Ridley, T., Pugh, S. A., Wilson, A. M., Waddell, K. L., and Conkling, B. L.: The Forest Inventory and Analysis Database: Database description and user guide version 6.0.2

for Phase 2. U.S. Department of Agriculture, Forest Service. 748 p. [Online]. Available at web address: http://www.fia.fs.fed.us/library/database documentation/, 2015.

Odum, E. P.: The strategy of ecosystem development. *Science* 164:262-270, 1969.

Pan, Y., Chen, J. M., Birdsey, R., McCullough, K., He, L, and Deng, F.: Age structure and disturbance legacy of North American forests. *Biogeosciences*, 8, 715-732, doi:10.5194/bg-8-715-2011, 2011a.

Pan, Y., Birdsey, R. A., Fang, J., Houghton, R., Kauppi, P. E., Kurz, W. A., Phillips, O. L., Shvidenko, A., Lewis, S. L., Canadell, J. G., Ciais, P., Jackson, R. B., Pacala, S. W., McGuire, A. D., Piao, S., Rautiainen, A., Sitch, S., and Hayes, D.: A large and persistent carbon sink in the world's forests. *Science*, 333, 988-993, 2011b.

Pimm, S. L.: The complexity and stability of ecosystems. *Nature*, 307, 321-326, 1984.

Pongratz, J., Reick, C. H., Houghton, R. A., and House, J. I.: Terminology as a key uncertainty in net land use and land cover change carbon flux estimates. *Earth System Dynamics*, 5, 177-195, doi:10.5194/esd-5-177-2014, 2014.

Potter, C., Tan, P.-N., Steinbach, M., Klooster, S., Kumar, V., Myneni, R., and Genovese, V.: Major disturbance events in terrestrial ecosystems detected using global satellite data sets. *Global Change Biology*, 9, 1005-1021, 2003.

Poulter, B., Frank, D., Ciais, P., Myneni, R. B., Andela, N., Bi, J., Broquet, G., Canadell, J. G., Chevallier, F., Liu, Y. Y., Running, S. W., Sitch, S., and van der Werf, G. R.: Contribution of semi-arid ecosystems to interannual variability of the global carbon cycle. *Nature*, 509, 600-603, doi:10.1038/nature13376, 2014.

Pretzsch, H., and Biber, P.: A re-evaluation of Reineke's Rule and stand density index. *Forest Science*, 51, 304-320, 2005.

Pretzsch, H., Grote, R., Reineking, B., Rötzer, TH., and Seifert, ST.: Models for Forest Ecosystem Mangement: A European Perspective. *Annals of Botany*, 101, 1065-87, doi:10.1093/aob/mcm246, 2008.

Pugh, T. A. M., Lineskog, M., Smith, B., Poulter, B., Arneth, A., Haverd, V., and Calle, L.: Role of forest regrowth in global carbon sink dynamics. *Proceedings of the National Academy of Sciences of the United States of America*, doi:10.1073/pnas.1810512116, 2019a.

Pugh, T. A. M., Arneth, A., Kautz, M., Poulter, B., and Smith, B.: Important role of forest disturbances in the global biomass turnover and carbon sinks. *Nature Geoscience*, 12, 730-735, doi: 10.1038/s41561-019-0427-2, 2019b.

Pütz, S., Groeneveld, J., Alves, L. F., Metzger, J. P., and Huth, A.: Fragmentation drives tropical forest fragments to early successional states: A modelling study for Brazilian Atlantic forests. *Ecological Modelling*, 222, 1986-1997, doi: 10.1016/j.ecolmodel.2011.03.038, 2011.

https://doi.org/10.5194/gmd-2020-258
Preprint. Discussion started: 22 September 2020

Reichstein, M., Bahn, M., Ciais, P., Frank, D., Mahecha, M. D., Seneviratne, S. I., Zscheischler, J., Beer, C., Buchmann, N., Frank, D. C., Papale, D., Rammig, A., Smith, P., Thonicke, K., van der Velde, M., Vicca, S., Walz, A., and Wattenbach, M.: Climate extremes and the carbon cycle. *Nature*, 500, 287-295, doi:10.1038/nature12350, 2013.

Ryan, M. G., Binkley, D., Fownes, J. H., Giardina, C. P., and Senock, R. S.: An experimental test of the causes of forest growth decline with stand age. *Ecological Monographs*, 74, 393-414, 2004.

Schaphoff, S., von Bloh, W., Rammig, A., Thonicke, K., Biemans, H., Forkel, M., Gerten, D., Heinke, J., Jägermeyr, J., Knauer, J., Langerwisch, F., Lucht, W., Müller, C., Rolinski, S., and Waha, K.: LPJmL4 – a dynamic global vegetation model with managed land – Part 1: Model Description. *Geoscientific Model Development*, 11, 1343-1375, 2018.

Shevliakova, E., Pacala, S. W., Malyshev, S., Hurtt, G. C., Milly, P. C. D., Caspersen, J. P., Sentman, L. T., Fisk, J. P., Wirth, C., and Crevoisier, C.: Carbon cycling under 300 years of land use change: Importance of the secondary vegetation sink. *Global Biogeochemical Cycles*, 23, GB2022, doi:10.1029/2007GB003176, 2009.

Sitch, S., Smith, B., Prentice, I. C., Arneth, A., Bondeau, A., Cramer, W., Kaplan, J. O., Levis, S., Lucht, W., Sykes, M. T., Thonicke, K., and Venevsky, S.: Evaluation of ecosystem dynamics, plant geography and terrestrial carbon cycling in the LPJ dynamic global vegetation model. *Global Change Biology*, 9, 161-185, 2003.

Stephenson, N. L., Das., A. J., Condit, R., Russo, S. E., Baker, P. J., Beckman, N. G., Coomes, D. A., Lines, E. R., Morris, W. K., Rüger, N., Alvarez, E., Blundo, C., Bunyavejchewin, S., Chuyong, G., Davies, S. J., Duque, A., Ewango, C. N., Flores, O., Franklin, J. F., Grau, H. R., Hao, Z., Harmon, M. E., Hubbell, S. P., Kenfack, D., Lin, Y., Makana, J.-R., Malizia, A., Malizia, L. R., Pabst, R. J., Pongpattananurak, N., Su, S.-H., Sun, I-F., Tan, S., Thomas, D., van Mantgem, P. J., Wang, X., Wiser, S. K., and Zavala, M. A.: Rate of tree carbon accumulation increases continuously with tree size. *Nature*, 507, 90-93, doi:10.1038/nature12914, 2014.

Stocker, B. D., Feissli, F., Strassmann, K. M., Spahni, R., and Joos, F.: Past and future carbon fluxes from land use change, shifting cultivation and wood harvest. *Tellus B*, 66, 23188, doi: 10.3402/tellusb.v66.23188,2014.

Thonicke, K., Venevsky, S., Sitch, S., and Cramer, W.: The role of fire disturbance for global vegetation dynamics: coupling fire into a Dynamic Global Vegetation Model. *Global Ecology & Biogeography*, 10, 661-677, 2001.

Tilman, D., and Downing, J. A.: Biodiversity and stability in grasslands. *Nature*, 367, 363-365, 1994.

Turner, M. G.: Disturbance and landscape dynamics in a changing world. *Ecology*, 91, 2833-2849, 2010.

van der Werf, G. R., Randerson, J. T., Giglio, L., van Leeuwen, T. T., Chen, Y., Rogers, B. R., Mu, M., van Marle, M. J. E., Morton, D. C., Collatz, G. J., Yokelson, R. J., and Kasibhatla, P. S.: Global fire emissions estimates during 1997-2016. *Earth System Science Data*, 9, 697-720, doi: 10.5194/essd-9-697-2017, 2017.

Williams, C A., Gu, H., MacLean, R., Masek, J. G., and Collatz, G. J.: Disturbance and the carbon balance of US forests: A quantitative review of impacts from harvests, fires, insects, and droughts. *Global and Planetary Change*, 143, 66-80, doi: 10.1016/j.gloplacha.2016.06.002, 2016.

Yue, C., Ciais, P., Luyssaert, S., Li, W., McGrath, M. J., Chang, J., and Peng, S.: Representing anthropogenic gross land use change, wood harvest and forest age dynamics in a global vegetation model ORCHIDEE-MICT v8.4.2. *Geoscientific Model Development*, 11, 409–428, doi: 10.5194/gmd-11-409-2018, 2018.

Xia, J., Luo, Y., Wang, Y.-P., and Hararuk, O.: Traceable components of terrestrial carbon storage capacity in biogeochemical models. *Global Change Biology*, 19, 2104–16, 2013.

https://doi.org/10.5194/gmd-2020-258
Preprint. Discussion started: 22 September 2020

Geoscientific Model Development Discussions

Table 1. Age-class widths corresponding to two different simulation age-class setups in LPJ. The age-class codes are referenced in Figures.

	Age-Widths (years)	
Code	**Unequal Bins**	**10-yr Equal Bins**
1	1-2	1-10
2	3-4	11-20
3	5-6	21-30
4	7-8	31-40
5	9-10	41-50
6	11-15	51-60
7	16-20	61-70
8	21-25	71-80
9	26-50	81-90
10	51-75	91-100
11	76-100	101-150
12	+101	+151

https://doi.org/10.5194/gmd-2020-258
Preprint. Discussion started: 22 September 2020

Geoscientific Model Development Discussions
Open Access EGU

Table 2. Description of LPJ-wsl simulations in this study, corresponding objectives and related science questions. Land Use Change and Land Management (LUCLM, LU).

Simulation	Description	Objective and Questions	*Structure/Processes Included* Age-classes	Fire	LUCLM
Single-cell					
S_{age_event}	Idealized simulations of a deforest, abandon, and regrow event. British Columbia, CAN [121.25W 57.25N]	Evaluate recovery dynamics of a single regrow event. Do age dynamics influence relaxation times?	✓	✓	✓
S_{noage_event}			*x*	✓	✓
Regional					
$S_{unequalbin}$*	Idealized simulation with 5% of grid-cell cleared annually to create a wide age-class distribution in mixed broadleaf and evergreen temperate forests of Michigan (MI), Minnesota, and Wisconsin (WI) of U.S.A.	Does the model capture 'classic' demographic patterns in stand structure (tree density and height) and function (NEP, NPP, Rh)?	✓*	*x*	*x*
$S_{10yrbin}$‡			✓‡	*x*	*x*
Global					
S_{noage}	Standard-forcing factorial simulations at global scale.	Do age dynamics influence global stocks and fluxes?	*x*	✓	✓
S_{Fire}		What is the relative contribution of Fire and LU to ecosystem age?	✓	✓	*x*
S_{LU}		Are demographic effects evident in fluxes, and where is the effect greatest?	✓	*x*	✓
S_{FireLU} (S_{age})		What is the relative contribution of climate versus demography on fluxes?	✓	✓	✓

* unequal age-width simulation. Age-widths as described in Table 1
‡ 10-yr interval age-width simulation. Age-widths as described in Table 1

https://doi.org/10.5194/gmd-2020-258
Preprint. Discussion started: 22 September 2020

Geoscientific Model Development
Discussions

Table 3. Linear trend statistics by zonal band from LPJ-wsl simulations, based on model (age = $\beta 0$ + $\beta 1$*year) where year at 1860 is indexed at 1. Coefficients listed as $\mu \pm$ S.E. All d.f. are 113 and $p < 0.001$.

Zonal Band	Simulation	$\beta 0$	$\beta 1$	R^2
Boreal	Fire Only (**S_{Fire}**)	141.7 ± 0.01	-0.0098 ± 0.0002	0.95
	Fire and LUCLM (**S_{FireLU}**)	139.7 ± 0.13	-0.0388 ± 0.0019	0.78
Temperate	Fire Only (**S_{Fire}**)	118.5 ± 0.05	-0.0525 ± 0.0008	0.98
	Fire and LUCLM (**S_{FireLU}**)	112.6 ± 0.21	-0.1383 ± 0.0032	0.94
Tropics	Fire Only (**S_{Fire}**)	95.9 ± 0.06	-0.0429 ± 0.0009	0.95
	Fire and LUCLM (**S_{FireLU}**)	88.9 ± 0.16	-0.1382 ± 0.0024	0.97

https://doi.org/10.5194/gmd-2020-258
Preprint. Discussion started: 22 September 2020

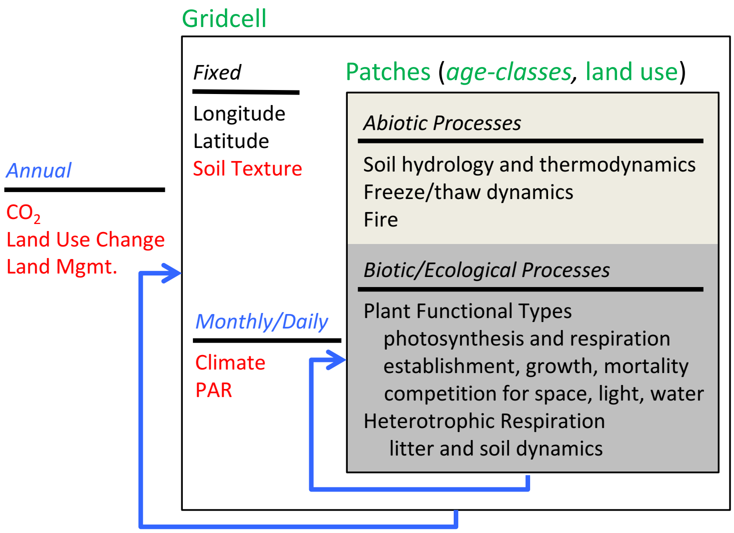

925 **Figure 1. LPJ-wsl model structure of inputs (red), time-steps (blue) and the level at which state variables are tracked within grid-cells and sub-grid-cell patches (green), such as age-classes or land uses. Simulation of abiotic, biotic and ecological processes occurs at the scale of a patch.**

https://doi.org/10.5194/gmd-2020-258
Preprint. Discussion started: 22 September 2020

Geoscientific Model Development
Discussions
Open Access
EGU

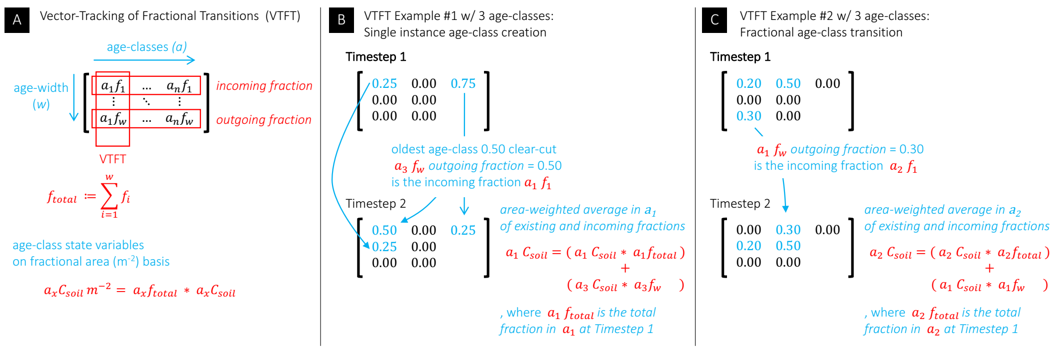

Figure 2. Methodological examples of the matrix based method called Vector-Tracking of Fractional Transitions for computationally-efficient simulation of age-classes in large-scale models. (a) Hypothetical matrix of VTFT vectors of fractional areas (*f*). The total area of the age-class is the sum of the fractional areas in the corresponding VTFT vector. State variables are calculated on area basis by accounting for the fractional area of the age-class, in this example C_{soil} is the carbon in soil. (b) An example of the VTFT method for a newly created age-class by clear-cut wood harvest. An area-weighted average updates age-class state variables in the youngest age-class using the preceding total fractional area of the age-class and the incoming fraction. (c) A VTFT example for a fractional age-class transition. An area-weighted average updates state variables in an age-class using the preceding total fractional area of the age-class and the incoming fraction from the younger age-class.

Geoscientific Model Development
Discussions
Open Access
EGU

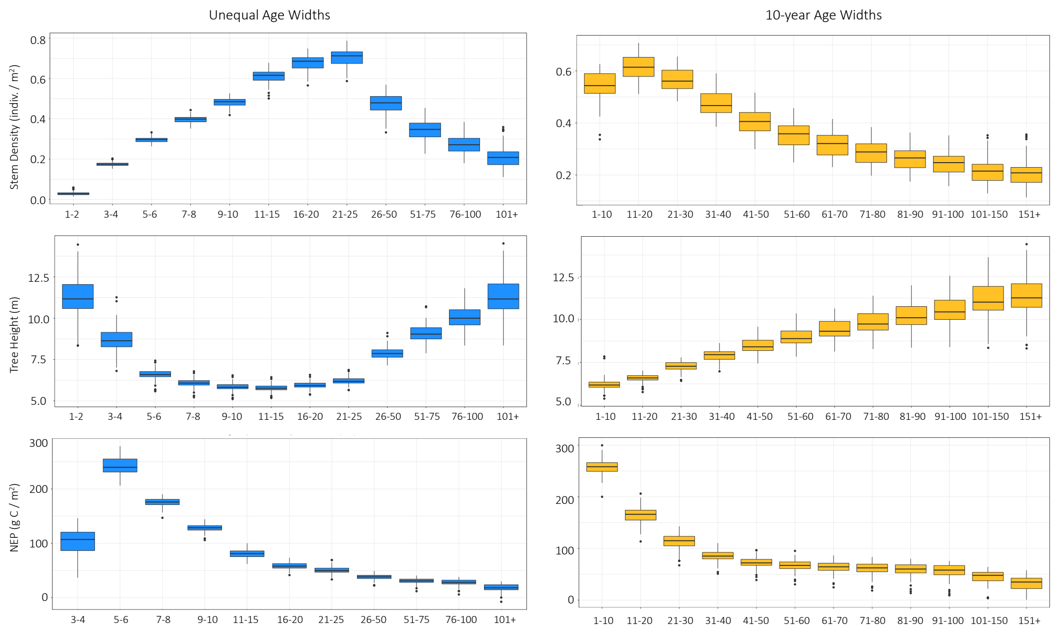

Figure 3. Boxplots by age-classes (x-axis, *in years*) from LPJ-wsl simulations for MI, MN, WI. (blue, left) Age-classes defined with *unequalbin* age widths (Table 1); small age-widths in the youngest age-classes towards progressively larger width age classes. Density peaks in the 21-25 year age-class and NEP peaks in the 5-6 year age-class. For average tree height (middle row), large tree height in the youngest age-class represents the 'survivor' trees; average tree height decreases as the density of establishing saplings increases. (gold, right) Age-classes in *10-yr-equalbin* age-widths (Table 1), the standard age-class setup used in global age-class simulations. Peaks in Density and NEP roughly follow the age-class patterns when finer age-widths are employed (blue, left).

https://doi.org/10.5194/gmd-2020-258
Preprint. Discussion started: 22 September 2020

Geoscientific Model Development
Discussions
Open Access

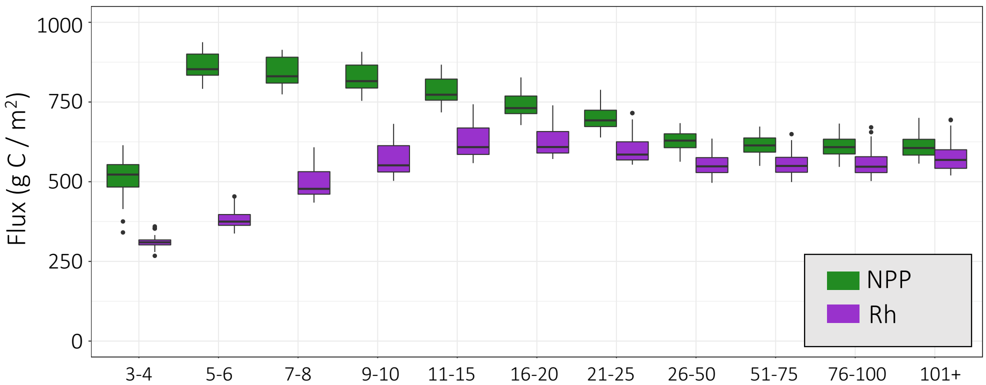

Figure 4. Boxplots of NPP and Rh by age-classes (x-axis, *in years*) from LPJ-wsl simulations for U.S. States MI, MN, WI. Age-classes defined with *unequalbin* age widths (Table 1); small age-widths in the youngest age-classes towards progressively larger age-widths.

https://doi.org/10.5194/gmd-2020-258
Preprint. Discussion started: 22 September 2020

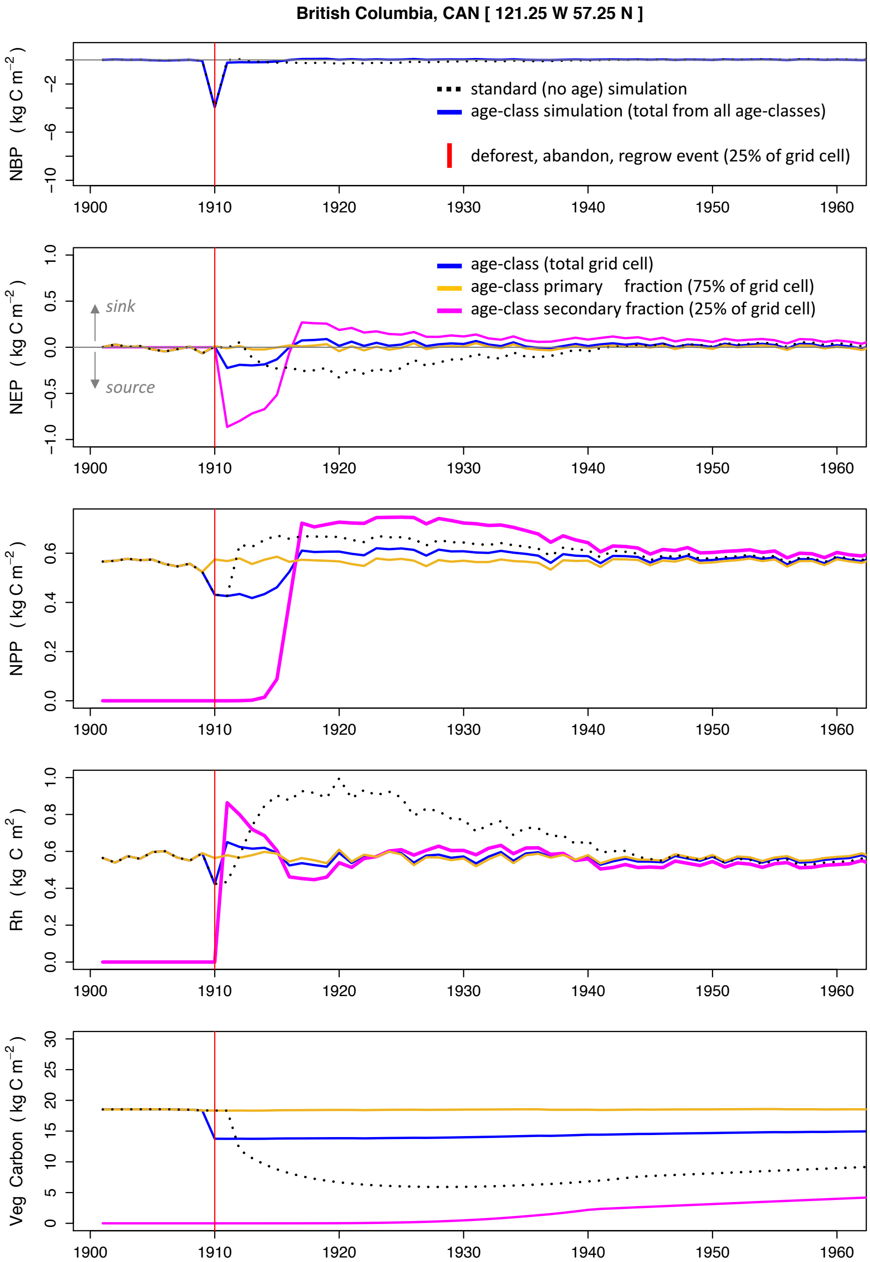

Figure 5. A time-series comparison between the standard LPJ-wsl simulation (S_{noage_event}) and the age-class approach (S_{age_event}) in an idealized single-cell simulation of a deforestation, abandonment, and subsequent regrow event. x-axis is the simulation year. See Table 2 for simulation details.

960

https://doi.org/10.5194/gmd-2020-258
Preprint. Discussion started: 22 September 2020

Geoscientific Model Development Discussions

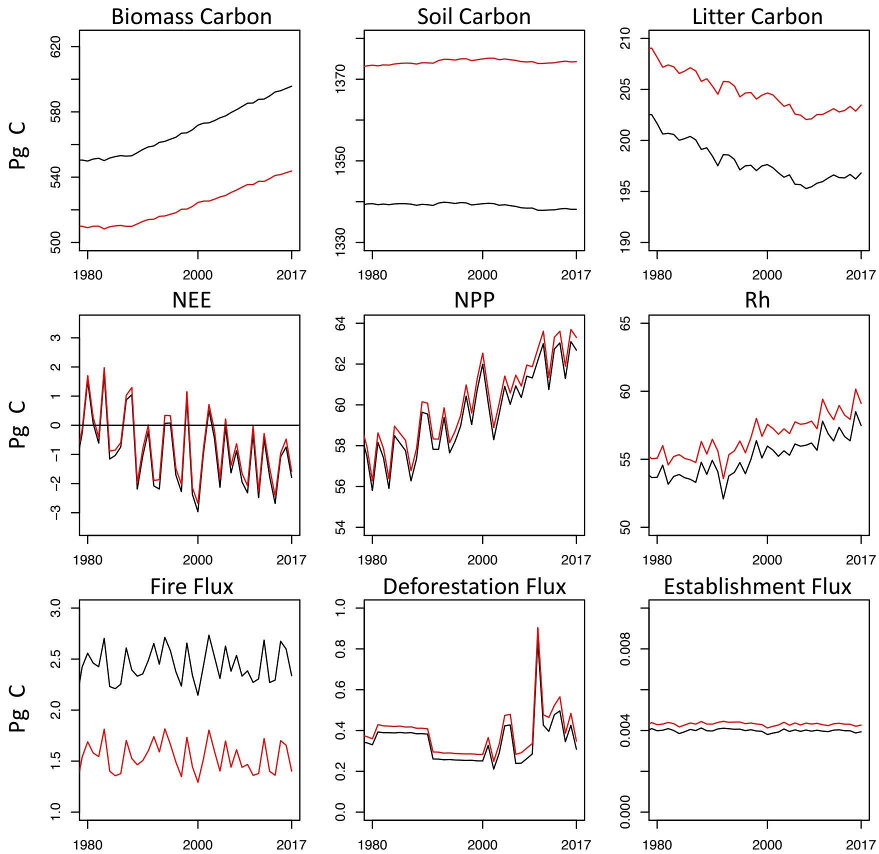

Figure 6. Time-series of global carbon stocks and fluxes from LPJ-wsl simulation *without* age-classes (black lines) compared against simulations *with* age-classes (red).

https://doi.org/10.5194/gmd-2020-258
Preprint. Discussion started: 22 September 2020

Geoscientific Model Development
Discussions
Open Access
EGU

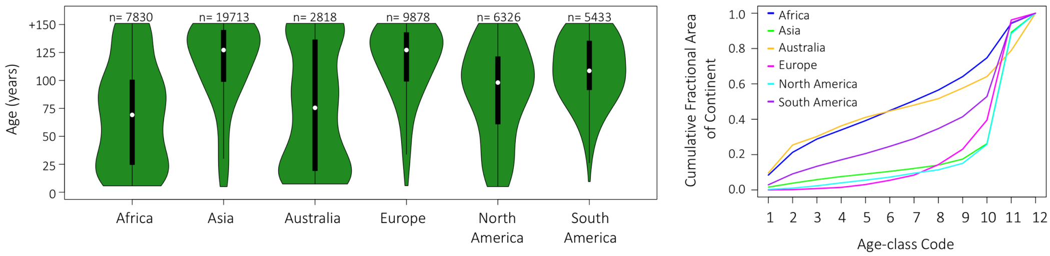

Figure 7. Age-class distributions by Continent. (left) Violin plots of ecosystem age by continent averaged over 2000-2010, based on LPJ-wsl simulations. Violin plots show the distribution of data points (green), interquartile range (black box) and the median value (white circle). The number of vegetated 0.5° grid-cells in each continent are above plot. (right) Cumulative fractional area in continent by age-classes. Age-class codes, lowest (youngest) to greatest (oldest), correspond to the *10-yr-equalbin* age-class setup (Table 1).

https://doi.org/10.5194/gmd-2020-258
Preprint. Discussion started: 22 September 2020

Geoscientific Model Development Discussions
Open Access

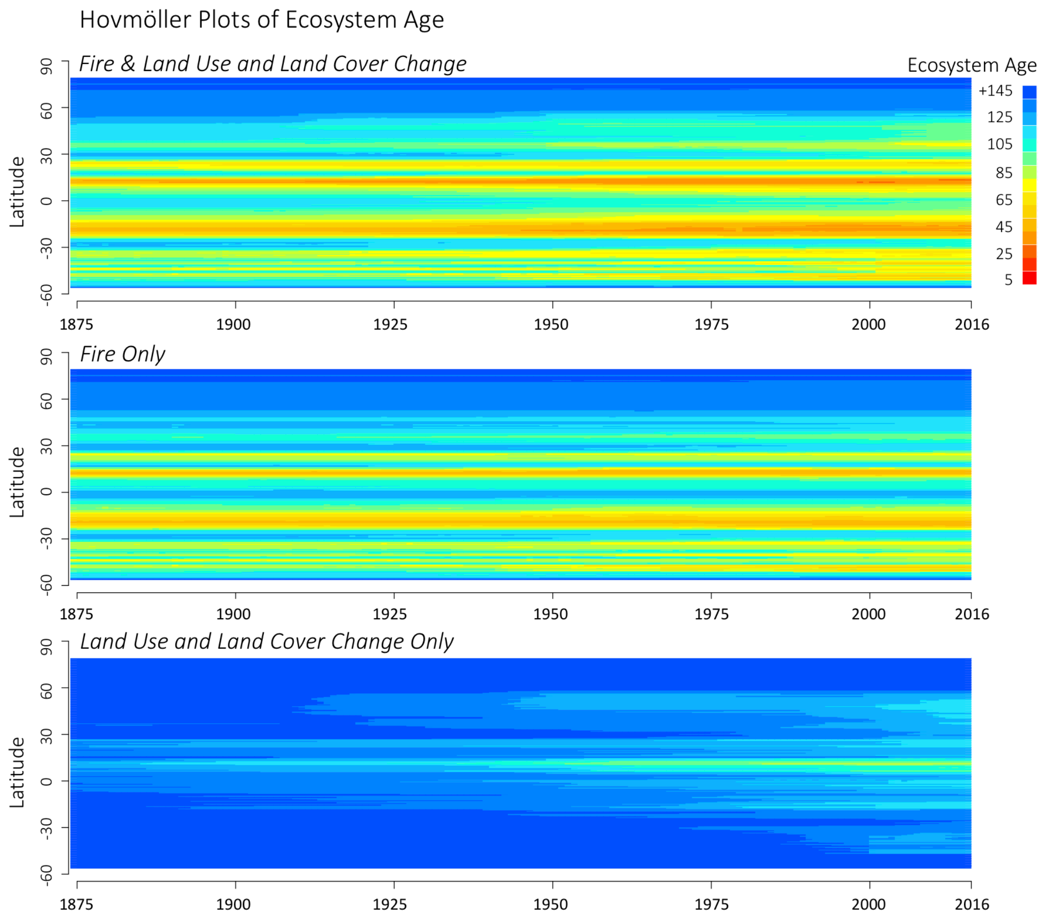

Figure 8. Zonal ecosystem age versus year based on LPJ-wsl simulations using full forcing (top), only fire (middle), or only land use and land cover change (bottom).

975

https://doi.org/10.5194/gmd-2020-258
Preprint. Discussion started: 22 September 2020

Geoscientific Model Development
Open Access
Discussions

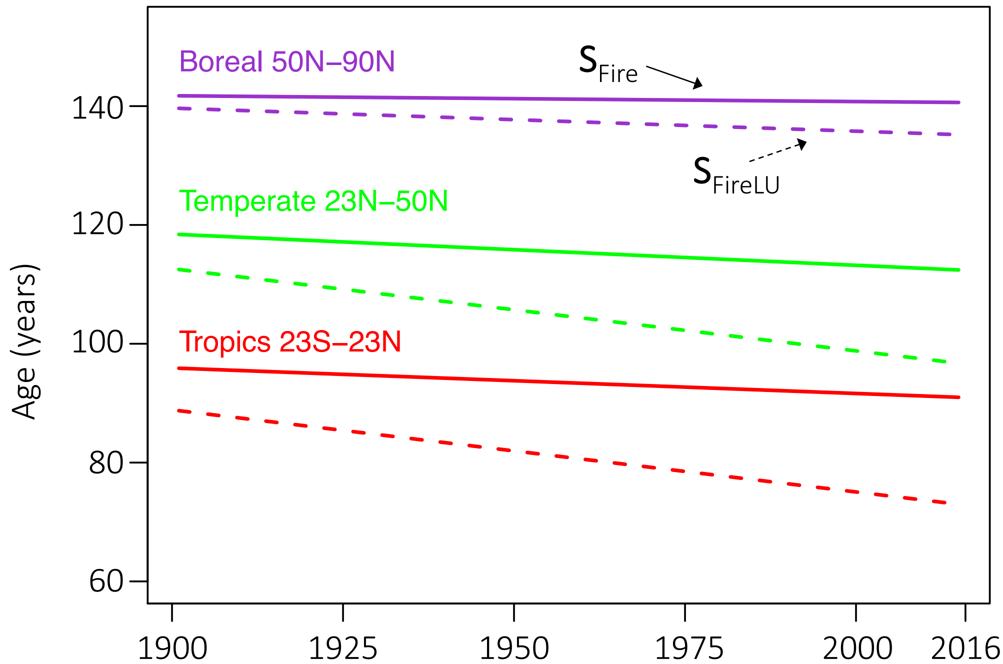

Figure 9. Trend in ecosystem age by zonal band for LPJ-wsl simulation with only fire (S_{Fire}, solid lines) and with both fire and LUCLM (S_{FireLU}, dashed lines). Fire causes zonal bands to differ in ecosystem age by ~23 years, and decreases the average age by 0.009 to 0.054/yr. LUCLM decreased ecosystem age at rates up to 3-times the rate of fire, from 0.038/yr in boreal zones to 0.138/yr in temperate and tropical zones.

https://doi.org/10.5194/gmd-2020-258
Preprint. Discussion started: 22 September 2020

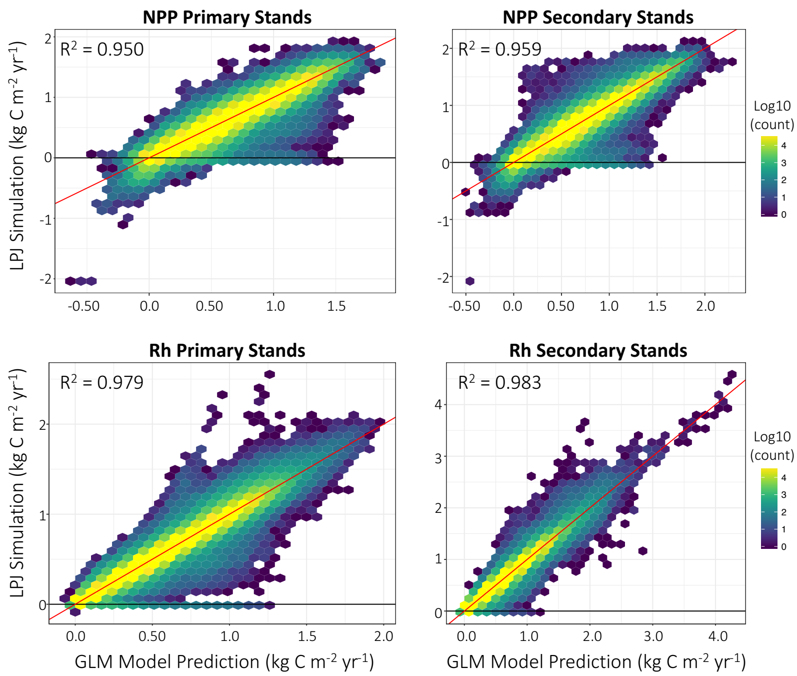

Figure 10. Annual fluxes (NPP, Rh) (2000-2017) from LPJ-wsl simulations versus predictions of LPJ-wsl fluxes based on a generalized linear model (flux = precipitation + temperature + age-class); coefficients were allowed to vary by grid-cell, in essence, reducing the effect of variation in plant composition, soil texture and hydrology. Coloring is by density of grid-cells on a log scale; diagonal red line is the 1:1 correspondence line. The simplified statistical model is can simplify the dynamics in the global vegetation model, with coefficients from the GLM helping to determine the relative importance of a small set of predictors.

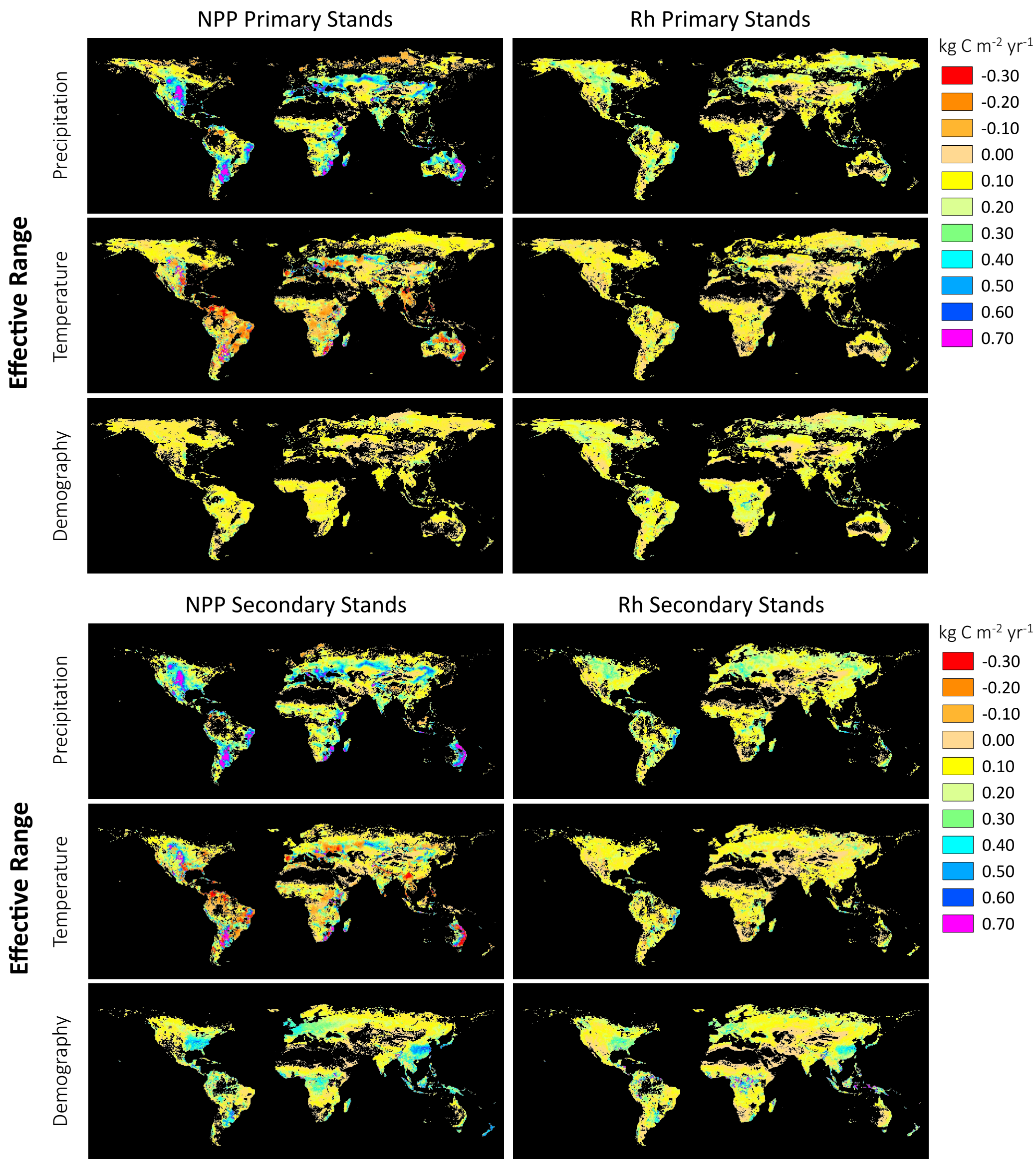

Figure 11. Global maps of the Effective Range of the Predictors (precipitation, temperature, demography) on LPJ-wsl fluxes (NPP, Rh); black is zero values or no-data. The Effective Range of the predictor is calculated as the grid-cell-specific beta (ß) coefficient multiplied by the observed range of the predictor variable for the
995 **grid-cell, for years 2000-2017. Units are on the scale of the predicted flux (kg C m^{-2} yr^{-1}). In these maps, an emphasis is placed on the effective range of the predictor rather than the absolute value of the coefficient, although these too can be mapped for forecasting purposes. See *Sect 2.3.6* and *Sect 3.4* for additional details.**

https://doi.org/10.5194/gmd-2020-258
Preprint. Discussion started: 22 September 2020

Geoscientific Model Development
Discussions

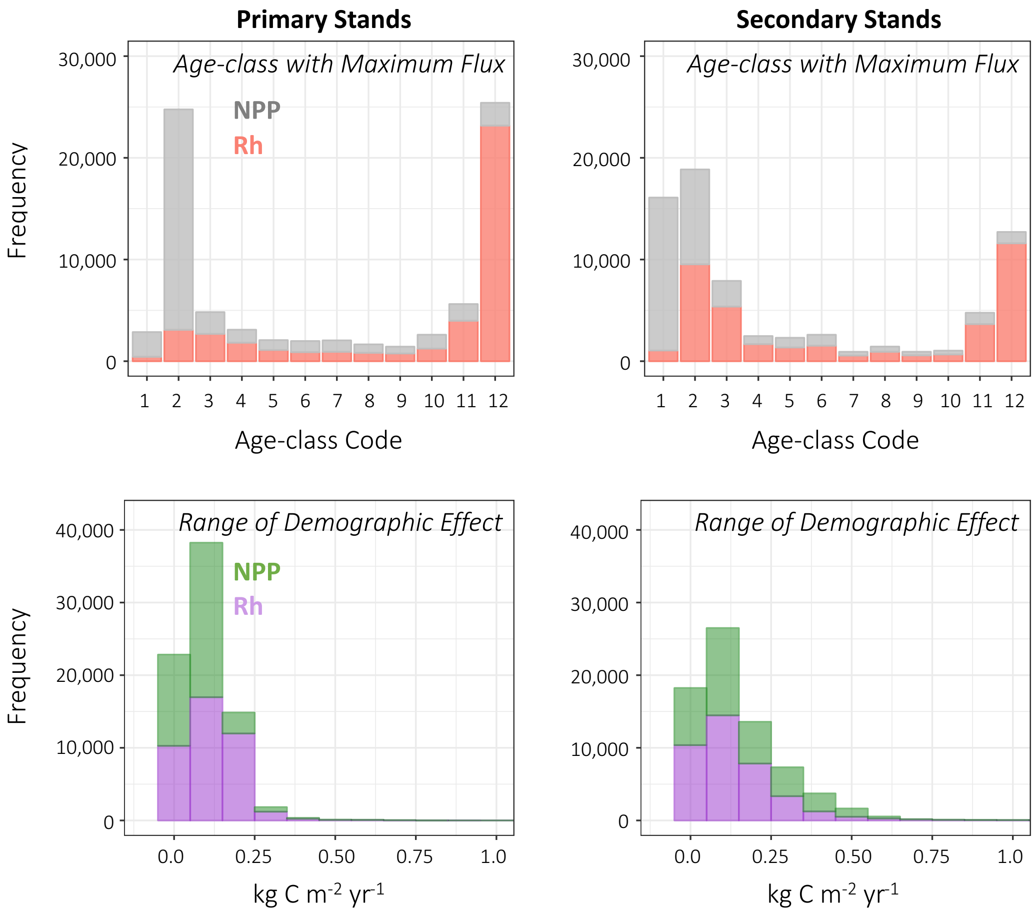

Figure 12. Stacked frequency plots for NPP, Rh on primary and secondary stands. (top row) Global frequency of age-classes with the largest flux (NPP, Rh), relative to other age-classes in the grid-cell. Age-class codes, lowest (youngest) to greatest (oldest), correspond to the *10-yr-equalbin* age-class setup (Table 1). (bottom row) Global frequency of the range of the demographic effect on fluxes, bin width is 0.10 kg C m^{-2} yr^{-1}. An example interpretation, on primary stands, (top left) NPP is greatest in the second age-class and (bottom left) the demographic effect on NPP is < 0.25 kg C m^{-2} yr^{-1}.

Geoscientific Model Development
Open Access
Discussions

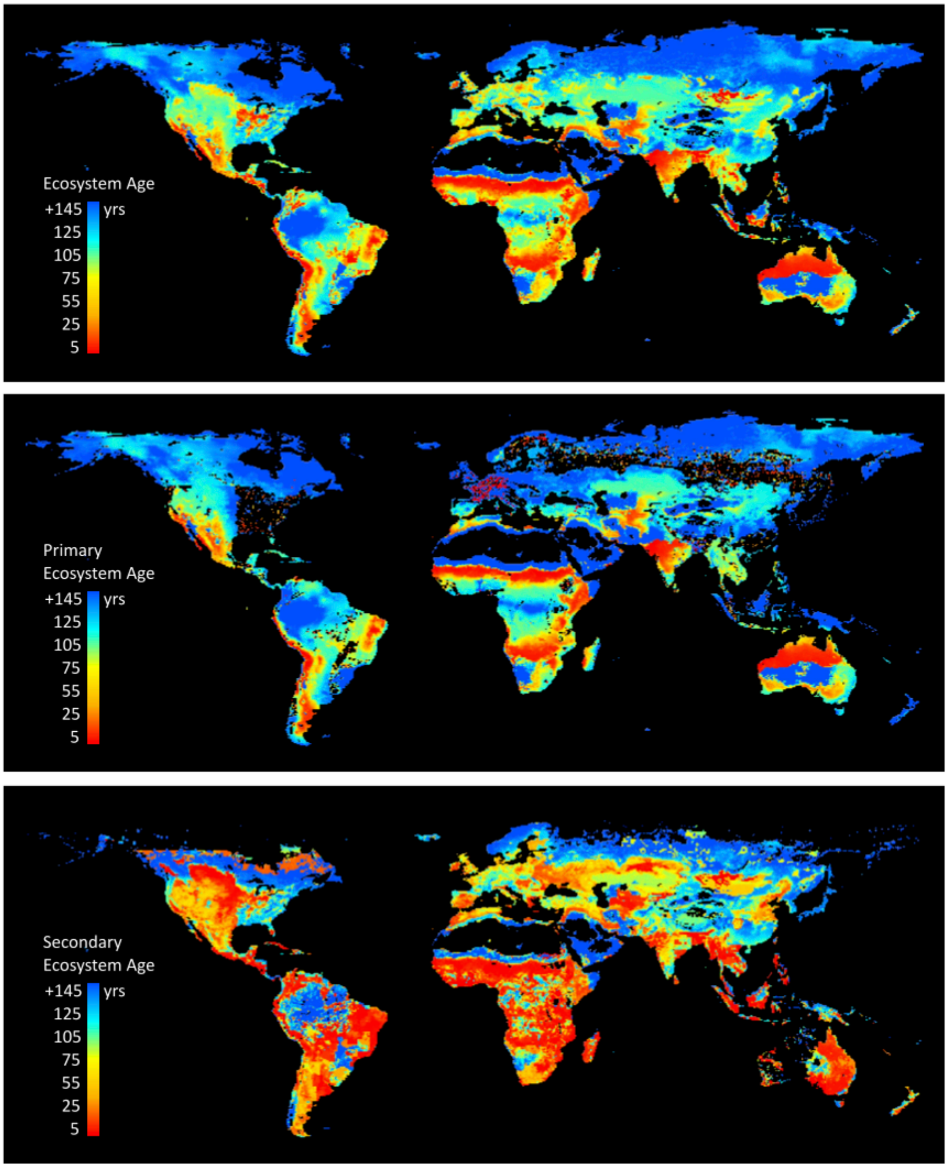

Figure 13. LPJ-wsl simulated global distribution of ecosystem ages, defined as the time since disturbance by fire and/or land use change and land management (LUCLM) in year 2016. (top) Average age of the natural ecosystem, scaled to the area of natural lands within 0.5° grid-cells. (middle) Average age of primary Ecosystems only, wherein only fire creates age structure, scaled to the area of primary lands. (bottom) Average age of secondary Ecosystems only, wherein fire and LUCLM creates age structure, scaled to the area of secondary lands.